NASA Technical Paper 3092

May 1991

Ground Effects on the Low-Speed Aerodynamics of a Powered, Generic Hypersonic Configuration

Gregory M. Gatlin

NASA

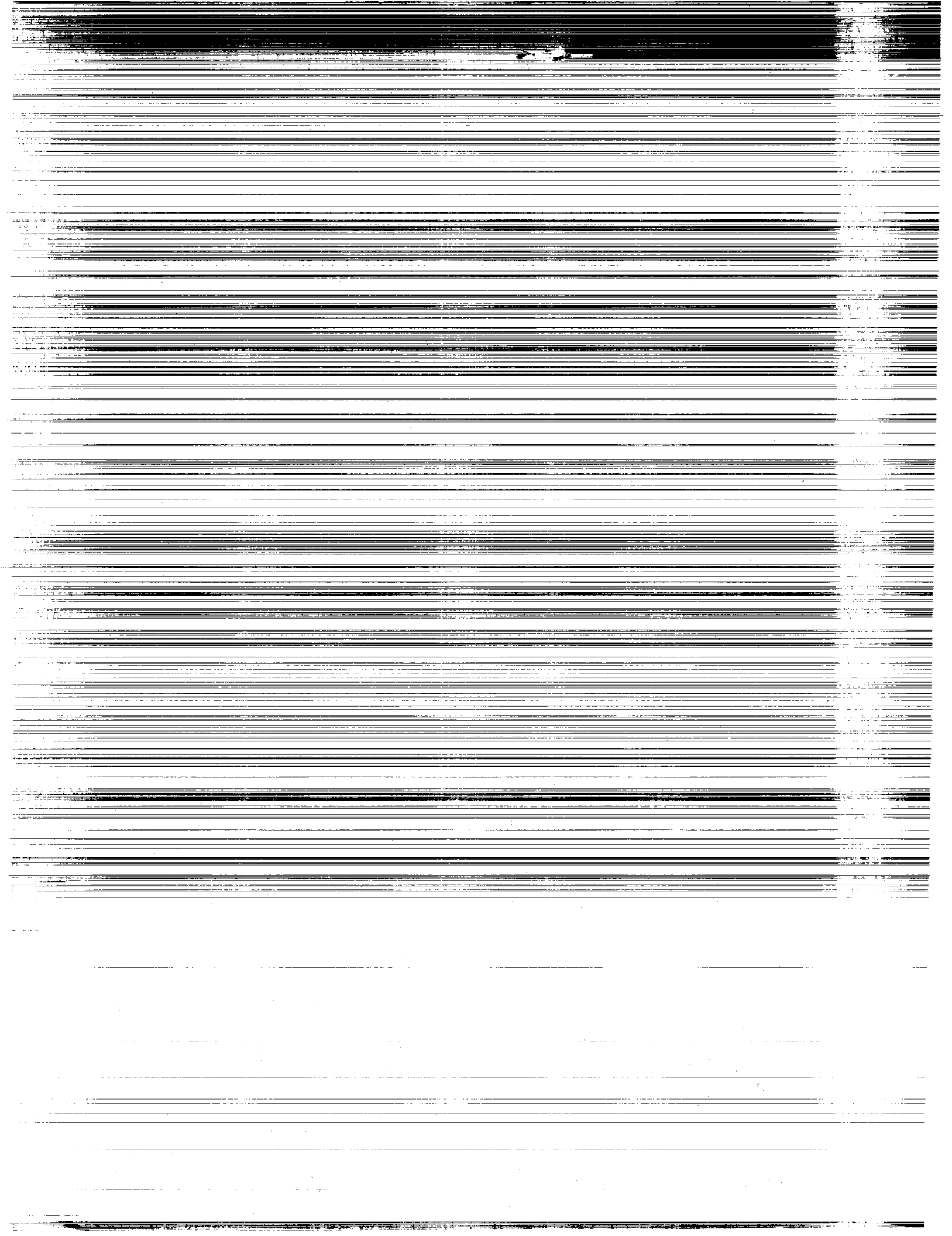

NASA Technical Paper 3092

1991

Ground Effects on the Low-Speed Aerodynamics of a Powered, Generic Hypersonic Configuration

Gregory M. Gatlin
Langley Research Center
Hampton, Virginia

NASA
National Aeronautics and Space Administration
Office of Management
Scientific and Technical Information Division

Summary

A study was undertaken in the NASA Langley 14- by 22-Foot Subsonic Tunnel to determine the low-speed aerodynamic characteristics of a powered, generic hypersonic configuration in and out of ground effect. The model was a simplified configuration consisting of a triangular-wedge forebody, a rectangular midsection that housed the flow-through, ejector-type propulsion simulation system, and a rectangular-wedge afterbody. Additional model components included a delta wing, a rectangular-wedge forebody, inlet fences, exhaust flow deflectors, and afterbody fences. Aerodynamic force and moment data were obtained over an angle-of-attack range from $-4°$ to $18°$ while the model height above the tunnel floor was varied from 1/4 in. to 6 ft. Variations in free-stream dynamic pressure, from 10 to 80 psf, and in engine ejector pressure yielded a range of thrust coefficients from 0 to 0.8.

Flow visualization studies were conducted in which water was injected into the engine simulator inlets and a laser light sheet was used to illuminate the resulting exhaust flow. In addition, surface oil flow visualization studies were used to determine the flow conditions on the forebody in the vicinity of the engine inlets. These techniques allowed diagnostic analysis of the undersurface forebody and exhaust flows and aided in interpreting the force and moment data.

Constraining the engine simulator flow field (both inlet and exhaust flows) between the large undersurface of the configuration and the tunnel floor produced significant power-on ground effects. Where lift increased with decreasing ground height during power-off testing, significant lift losses were noted in ground effect as thrust was increased. Variations in angle of attack as well as the presence of afterbody fences also had a substantial influence on the ground effects during power-on testing. A control surface on the undersurface of the afterbody could effectively deflect the exhaust flow for longitudinal control, and inlet fences eliminated the spanwise flow in the vicinity of the inlet plane. Further results indicated that adding a wing to the configuration reduced, but did not eliminate, the power-on lift losses in ground effect. Both afterbody flap and wing flap deflections were influenced by power and were sensitive to ground effects.

Introduction

Renewed interest in hypersonic flight has developed with the current undertaking of the National Aero-Space Plane (NASP) Program. Particular emphasis has been placed on a single-stage-to-orbit vehicle with the ability to take off and land horizontally. Hypersonic flight requires long, slender configurations in which the propulsion system is a significant component that must be effectively integrated into the entire length of the vehicle (ref. 1). Thus the propulsion system will play a significant roll in the aerodynamics and performance of the vehicle throughout the flight regime. A substantial inlet flow as well as an extensive exhaust flow will be present on the undersurface of this type of configuration, thereby presenting the possibility for substantial ground effects during takeoff and landing operations. Since little is currently known about the low-speed aerodynamics of such configurations in the takeoff and landing regime, efforts are now underway to develop the data needed for the design of these advanced vehicles (ref. 2).

This paper presents highlights of two investigations conducted in the NASA Langley 14- by 22-Foot Subsonic Tunnel to study the ground effects on the low-speed aerodynamics of a hypersonic NASP-like configuration. The configuration consisted of a simplified fuselage with a flow-through, ejector-type propulsion simulation system. The forebody had a triangular planform with a wedge profile, the midsection was rectangular and housed the propulsion simulation system, and the afterbody had a rectangular planform with a wedge profile. The first investigation, also presented in reference 3, focused on basic concerns such as the effects of variations in thrust coefficient and angle of attack on overall configuration aerodynamics as the model was lowered into ground effect. In addition, some preliminary attempts were made to separate or deflect the exhaust flow away from the afterbody as a means of longitudinal control. The second investigation was developed from the results of the first investigation, but it was more detailed in that several geometric variations were studied. These included a rectangular-planform forebody, inlet fences, a faired inlet, a $70°$ delta wing (tested in two positions), and several exhaust-flow deflectors larger than those tested in the initial investigation.

In general, the investigations covered an angle-of-attack range from $-4°$ to $18°$, a dynamic pressure range from 10 to 80 psf, a thrust coefficient range from 0 to 0.8, and a model height range from 1/4 in. to 6 ft above the wind-tunnel floor. The majority of the tests were conducted at Reynolds numbers from 1.0×10^6 to 1.2×10^6 per foot. Data obtained included six-component forces and moments as well as surface flow and flow field visualization.

Symbols

All measurements are presented in U.S. Customary Units. All data have been reduced to standard coefficient form, and longitudinal data are presented in the stability axis system. The terms in parentheses are the symbols used in computer-generated data tables.

b		body span, ft
C_D	(CD)	drag coefficient, $\frac{\text{Drag}}{q_\infty S}$
C_L	(CL)	lift coefficient, $\frac{\text{Lift}}{q_\infty S}$
C_m	(CM)	pitching-moment coefficient, $\frac{\text{Pitching moment}}{q_\infty S \bar{c}}$
C_T	(CT)	thrust coefficient, $\frac{\text{Static thrust}}{q_\infty S}$
$\bar{c}$		mean geometric chord of body, ft
h/b	(H/B)	ratio of model height above tunnel floor to body span
q_∞	(Q)	free-stream dynamic pressure, $\frac{1}{2}\rho V_\infty^2$, psf
S		model planform reference area, ft^2
V_∞		free-stream velocity, ft/sec
$\dot{w}$	(W)	exit weight flow rate from engine simulation system, lb/sec
α	(ALPHA)	angle of attack, deg
δ_{ABF}		afterbody-flap-deflection angle, deg
δ_F		wing-flap-deflection angle, deg
ρ		density, $slugs/ft^3$

Abbreviations:

AB	afterbody
FB	forebody
F.T.	flow through
FWD	forward

Model Description

Baseline Configuration

The study of a generic hypersonic vehicle was conducted in two separate wind-tunnel entries. The model configurations and components for both entries will be described in this section. The baseline configuration, used in both investigations, consisted of a 9.4-ft-long by 2-ft-wide fuselage with rectangular cross sections and an engine simulation system consisting of eight engine units. A sketch of the model is shown in figure 1, and a photograph of the model mounted in the test section of the Langley 14- by 22-Foot Subsonic Tunnel is presented in figure 2. A list of pertinent model dimensions is presented in table I. The fully metric model was sting mounted on an internal, six-component strain-gauge balance with the support system entering the top of the model at a 37.5° angle relative to the model centerline. A balance fairing was implemented in this area to cover the top end of the balance and to provide a smooth free-stream flow over the upper surface of the afterbody. The forebody consisted of a wedge with a 10° undersurface ramp angle and had a triangular planform. The afterbody consisted of a wedge with a 14° undersurface ramp angle and had a rectangular planform. The midsection of the model housed the balance and two plenums for the high-pressure air-propulsion simulation system.

The propulsion simulation system consisted of eight flow-through engine units as sketched in figure 3. Each unit had a converging inlet duct, two high-pressure air injection tubes, and a diverging exhaust duct. This design not only entrained flow into the inlet but also mixed this inlet flow with the high-pressure ejector flow to provide exhaust flow for complete simulation of low-speed engine operations. High-pressure air was supplied to the model through a standard NASA air sting that contained a coiled air line to minimize interference effects between the high-pressure air line and the force balance. Details of the air sting are provided in reference 4.

First Investigation

In the first investigation, several add-on model components were tested in order to determine their effects on the longitudinal aerodynamics. These included exhaust flow deflectors, afterbody fences, and a 79° delta wing. Four different exhaust flow deflectors were tested to determine their suitability as a means of longitudinal control, and a sketch of each one is presented in figure 4. Three of the exhaust flow deflectors, which are referred to as "strips," were simply flat surfaces positioned perpendicular

to the afterbody lower surface and located 4 in. downstream from the exhaust nozzles. The three different heights tested for these strips were 0.375, 1, and 3 in. The 0.375-in. strip has a slightly different profile, as shown in figure 4, because of a different method of attachment. The fourth exhaust flow deflector tested was a 30° wedge strip that was 2.5 in. long and 1.5 in. high. It was located on the afterbody right at the position of the nozzle exhaust. Each of the exhaust flow deflectors spanned the entire width of the engine simulation system.

A sketch of the afterbody fences that were tested is presented in figure 5. The afterbody fences were the same height as the exit of the engine simulation system, i.e., 2.2 in. They were mounted flush with the sides of the engine simulation system, and they extended all the way to the trailing edge of the afterbody. These afterbody fences were tested in both wind-tunnel entries.

A sketch of the 79° delta wing that was tested on the configuration is presented in figure 6. The 79° delta wing consisted of a 0.25-in-thick flat plate mounted on the top of the fuselage. It had a 30° beveled leading edge and increased the model planform reference area by 35 percent over the baseline configuration.

Second Investigation

In the second investigation, the scope of the research was expanded and several additional model components were fabricated and tested based on results obtained from the first investigation. Some of these new components included a rectangular planform forebody, inlet fences, and a faired-over inlet in which a flat plate covered the inlet plane to eliminate all inlet flow into the engine simulation system. A sketch of the configuration tested with both the rectangular forebody and the inlet fences is presented in figure 7. The rectangular forebody maintained the 10° angle on the undersurface while also maintaining a 2-ft span along its entire length. Inlet fences, which were tested only on the rectangular forebody, were 1.5 in. tall, 32 in. long, and mounted flush with the outboard edges of the engine simulation system.

Another configuration consisting of a 70° delta wing, wing flaps, and an afterbody flap was also tested in the second investigation. The 70° delta wing had a 30° beveled leading edge and was tested in a forward and an aft position as illustrated in figure 8. The exposed wing area was 28 percent smaller, and both test positions were located farther aft on the configuration than the 79° delta wing tested in the first investigation. The wing flaps had a 6-in. chord and spanned the entire trailing edge of the wing. The afterbody flap also had a 6-in. chord and spanned the entire width of the afterbody. The wing and flaps were all flat plates that were ¼ in. thick.

The final set of configurations tested during the second wind-tunnel entry consisted of various exhaust flow deflectors mounted on the baseline configuration. These exhaust flow deflectors were wedge blocks that were much larger than the wedge strip tested in the first investigation. A sketch of these wedge-block exhaust flow deflectors is provided in figure 9. The new wedge blocks were 6 in. long and spanned the width of the engine simulation system. Wedge-block angles of 14°, 30°, and 45° were tested in a forward and an aft position as illustrated in the sketch in figure 9. Some data were also obtained with the 45° wedge block in the aft position in combination with the afterbody fences, as is also illustrated in figure 9.

Test Conditions and Techniques

Wind-Tunnel Description

The investigations were conducted in the NASA Langley 14- by 22-Foot Subsonic Tunnel. This facility is a closed-circuit, single-return, atmospheric wind tunnel capable of producing a maximum test section speed of 200 knots. A floor boundary-layer removal system is located at the entrance to the test section and is used for ground effects testing. Additional tunnel capabilities and a complete description of the facility are presented in reference 4.

Test Conditions

In the present investigations, testing was conducted at model heights above the tunnel floor from ¼ in. to 6 ft. The ground-height reference point on the model used to set the various heights was the lower trailing edge of the engine simulation system as identified in figure 1. Additional test parameters were thrust coefficients from 0 to 0.8, angles of attack from −4° to 18°, and free-stream dynamic pressures from 10 to 80 psf. An angle of attack of 12° was chosen as a value representative of takeoff and approach conditions, and thus was used for the majority of the ground effects data obtained. The moment reference center of the configuration was located 6 in. above the bottom of the model and at a distance back from the nose equal to 62 percent of the overall length of the baseline model (see fig. 1) for all configurations tested in both investigations.

The majority of the testing was conducted at free-stream dynamic pressures from 30 to 40 psf that correspond to Reynolds numbers from 1.0×10^6 to 1.2×10^6 per foot. At these dynamic pressures a

thrust coefficient of 0.4 was achieved using the maximum amount of engine thrust available. A thrust coefficient of 0.4 was chosen because it is a representative value of takeoff and approach conditions. The maximum pressure ratio of jet total pressure to free-stream static pressure (nozzle pressure ratio) that could be produced by the engine simulation system under these conditions was on the order of 1.1.

Test Techniques

Prior to the investigation a constant high-pressure air supply was applied to the model, and individual needle valves on the supply tube to each engine unit were adjusted to yield the same mass flow for each engine unit. This provided a uniform exhaust flow across the span of the engine simulation system.

The forces and moments on the configuration were measured with an internal six-component, strain-gauge balance. Even though all six force and moment components were measured, only the longitudinal components were of interest in this study. In both investigations, calibration of air line pressure tares was obtained prior to model buildup and appropriate corrections were made to the balance output.

In the first investigation, powered test conditions were run by setting the parameter thrust coefficient C_T. This was appropriate for configuration comparisons as long as there were no changes to the reference area S, since C_T is a function of S.

In the second investigation, the configurations had different reference areas, such as the rectangular-wedge forebody and delta wing configurations; thus C_T would not be an appropriate parameter to match when comparing these configurations. A more appropriate correlation parameter in this case would be the exit weight flow rate exhausting from the engine simulation system $\dot{w}$. This exit weight flow rate was calculated by adding the inlet flow rate and the high-pressure air ejector flow rate. The inlet flow rate was measured during the second investigation by pitot static probes mounted in the engine inlets. It should be noted that for the baseline configuration, an engine weight flow rate of 9 lb/sec was equivalent to a thrust coefficient of 0.4.

Flow visualization studies were conducted in both investigations. Separate techniques were used to visualize the flow on the model surface and in the flow field near the model. The surface flow visualization was obtained using a mixture of mineral oil, oleic acid, and titanium dioxide applied with a paint brush. This mixture was applied to the undersurface of the forebody to visualize the flow conditions in the vicinity of the engine inlets. The following procedure was used: the mixture was applied to the model surface, the model attitude and test conditions were held constant while the flow pattern was established, the tunnel was quickly brought to zero velocity, and then photographs were taken.

A water injection technique was used to visualize the location and behavior of the exhaust flow in the vicinity of the model. This was done by injecting water into each of the eight engine inlets such that the water would mix with the inlet flow and the high-pressure air exhaust flow. The mixture of water and air produced a dense water spray mist in the exhaust flow that was then clearly illuminated using a horizontal laser light sheet positioned parallel to the floor as illustrated in figure 10. The photographs presented using this technique show more detail on the right side of the model since the laser light sheet is being directed at the exhaust flow from that direction and its intensity has not yet been diminished by the density of the water mist as is the case on the left side of the model.

Presentation of Results

The results of both investigations are presented as follows. Test configurations are listed in table II, and the measured longitudinal force and moment data for all configurations are presented in coefficient form in table III. Graphical representations of the data presented as comparisons between specific configurations, along with flow visualization results, are presented in the following figures:

Discussion

Baseline Aerodynamics

This study was undertaken to determine the low-speed aerodynamic characteristics of a powered, generic hypersonic configuration in ground effect. The substantial inlet flow as well as the extensive exhaust flow present on the undersurface of this type of configuration led to a concern of substantial ground effects during takeoff and landing operations. The location and behavior of the exhaust flow was of prime importance in determining the ground effects; therefore exhaust flow visualization was conducted to gain further insight into this area. A flow visualization photograph is presented in figure 10 in which a laser light sheet was used to illuminate a water spray mist in the exhaust flow as explained earlier. The test conditions in the photograph were representative of takeoff and approach conditions. The photograph illustrates the significant region under the model influenced by the exhaust flow and highlights the concern that ground effects could be severe for hypersonic configurations.

In order to investigate the low-speed aerodynamic characteristics in ground effect, force and moment data were obtained at the representative takeoff and approach angle of attack of 12° (2° less than the nozzle expansion angle) for values of thrust coefficient ranging from 0 to 0.8. Most of this phase of the investigation was conducted at a free-stream dynamic pressure of 40 psf; however this limited the thrust coefficient to a maximum value of 0.4. Values of thrust coefficient greater than 0.4 were obtained by testing at free-stream dynamic pressures below 40 psf. Longitudinal aerodynamic data as a function of nondimensional model height (the ratio of model height above tunnel floor to body span) are presented for various power settings ranging from power off ($C_T = 0$) up to a thrust coefficient of 0.8 in figure 11. These data indicate conventional ground effects for the power-off condition as illustrated by increased lift with decreasing model height above the floor. However, this trend reversed as thrust was increased, and significant lift losses developed as the model was lowered into ground effect. Slight increases in both C_D and C_m were noted for both power-off and power-on conditions as the model was lowered into ground effect. All these effects were most apparent as the model was lowered below a height-to-body span ratio h/b of 0.5. A representative wheel touchdown height for this configuration would be at an h/b of approximately 0.08 (as denoted by the dashed lines in fig. 11). Thus, the observed ground effects would be within the operating range of the vehicle for takeoff and landing conditions.

Further investigations were conducted to determine how ground effects vary with angle of attack. Power-on ($C_T = 0.4$) longitudinal aerodynamic data, as the model was lowered into ground effect, are presented for angles of attack ranging from 8° to 14° in figure 12. At the angles of attack of 8°, 10°, and 12°, lift decreases at a rapidly increasing rate as the model is lowered below an h/b of 1.0. This is not the case for the angles of attack of 13° and 14°. As h/b is reduced down to a value of 0.05 for $\alpha = 13°$, the lift-loss trend is the same as that for the lower angles of attack; however at very low ground heights such as $h/b < 0.05$, there is a rapid lift increase. As h/b is reduced for $\alpha = 14°$, lift remains essentially constant until the very low ground heights are reached where there is again a rapid lift increase.

These power-on ground effects data show a very significant sensitivity to variations in angle of attack. More specifically, however, the adverse lift loss at the lower angles of attack in ground effect is removed and lift increases are observed as the angle of attack is increased to the order of the afterbody ramp angle. Thus, the rotation angle for takeoff and the angle of attack for approach may well be areas requiring careful consideration to avoid undesirable ground effects.

Inlet Flow Conditions

A smooth undisturbed inlet flow is critical to the performance of any airbreathing propulsion system. This condition, however, was not the case on the outboard engines as identified in the photograph presented in figure 13. This photograph is a close-up view of the engine inlets on the midsection of

the model with the forebody removed, and it shows streaks along the outboard side of the outboard engine-inlet splitter plates resulting from residue in the free-stream flow that accumulated throughout the duration of the first wind-tunnel investigation. These streaks identify areas of vortex flow, and therefore they reveal regions with a spanwise component of flow at the engine-inlet plane. This flow pattern was visible on all engine units except for the two engine units in the center of the configuration.

To further investigate spanwise flow conditions in the vicinity of the engine inlets, oil flow visualization studies were conducted on the undersurface of the forebody in the second investigation. Tests were performed to illustrate the effects of variations in ground height and angle of attack on the forebody flow conditions in the vicinity of the engine inlets. Three power-on test conditions are represented in the photographs in figure 14 to illustrate these effects. The first photograph (fig. 14(a)) reveals a spanwise flow on the forebody undersurface that increases with outboard spanwise location of the engine inlets. Thus, with the model out of ground effect at $\alpha = 12°$, there is some apparent spanwise flow in the region of the outboard engine inlets. The second photograph (fig. 14(b)) was taken at the same conditions, but with the model in ground effect. This photograph indicates an increased amount of spanwise flow on the forebody, particularly near the outboard inlets. The third photograph (fig. 14(c)) documents the lower-surface forebody flow field for the configuration in ground effect at $\alpha = -3.5°$, and it shows essentially no spanwise flow at the outboard inlets. Therefore, it appears that the greatest amount of spanwise flow on the forebody, under simulated powered conditions, occurs at positive angles of attack in ground effect.

A spanwise component of flow along the inlet plane of the outboard engines is certainly an undesirable inlet flow condition that will need to be addressed across the speed range for this class of vehicles. Since much of the spanwise flow was shown in figure 14 to occur near the outboard inlets, an attempt was made to minimize this spanwise flow by testing a set of inlet fences as illustrated in figure 7. Because of model constraints, the inlet fences could be tested only on the rectangular forebody; however similar effectiveness would be expected if the inlet fences were employed on the baseline configuration since the forebody flow fields appear to be identical in the vicinity of the inlet plane. (Compare figs. 14(b) and 15(a).) Surface oil flow visualization results illustrating the effectiveness of the inlet fences are presented in figure 15. The test conditions presented are for the configuration in ground effect at $\alpha = 12°$ with power on. The inlet flow visualization on the rectangular forebody without inlet fences is similar to that of the baseline configuration in that there is a significant amount of spanwise flow on the forebody. The configuration with the inlet fences, however, has a redirected forebody flow field in which the spanwise flow at the outboard inlets is completely eliminated. Thus, inlet fences effectively prevent spanwise flow on the forebody at the inlet plane at an angle of attack of 12° in ground effect.

Longitudinal aerodynamic data were obtained for the configuration with the rectangular forebody and are compared with the data for the baseline configuration in figure 16. Data are presented for both power-on ($\dot{w} = 9$ lb/sec) and power-off conditions as a function of nondimensional ground height. (Recall that for the baseline configuration, $\dot{w} = 9$ lb/sec is equivalent to $C_T = 0.4$.) These data are presented at a representative takeoff and approach angle of attack of 12°. The baseline configuration demonstrated conventional ground effects for the power-off condition as illustrated by increased lift with decreasing model height above the floor. However, this trend was reversed for the power-on condition previously illustrated in figure 11, and significant lift losses developed as the model was lowered into ground effect. The rectangular forebody configuration produced more lift than the baseline configuration under all conditions and reduced the magnitude of the power-on lift loss in ground effect. Slight increases in both C_D and C_m were noted for both configurations as the model was lowered into ground effect.

Longitudinal aerodynamic data for the rectangular forebody configuration with and without inlet fences are presented at an angle of attack of 12° in figure 17. These data show a lift loss and a corresponding increment in nose-down pitching moment when the inlet fences are added to the configuration during power-off conditions. When the power-on conditions are compared, the inlet fences create a lift loss in ground effect and, again, a corresponding increment in nose-down pitching moment. However, the inlet fences appear to have very little effect on drag during both power-off and power-on conditions. Thus, the rectangular-wedge forebody acts to reduce the significant power-on lift loss that is present with the baseline configuration, and the addition of inlet fences, in general, creates a lift-loss increment at the takeoff and approach angle of attack of 12°.

A further investigation of inlet flow conditions was conducted in which a faired-over inlet was tested to see how accurately it compared with the baseline flow-through inlet. The faired inlet was produced by

simply securing a flat plate over the inlet plane such that there would be no inlet flow. Forebody surface oil flow patterns are presented for both the baseline configuration and the faired-inlet configuration in figure 18. Both of the flow patterns were generated with the configuration at $\alpha = 12°$, the model at the approximate wheel touchdown height ($h/b = 0.08$), and the engine weight flow rate $\dot{w}$ set at 5 lb/sec. Engine weight flow rate was used as a correlating parameter because it was felt to be a more appropriate parameter to match in an inlet flow comparison than the thrust coefficient. A weight flow rate of 5 lb/sec was chosen since that was the maximum exhaust flow rate that could be produced with the inlet faired.

The flow visualization photograph for the flow-through inlet in figure 18(a) shows a component of spanwise flow on the forebody that increases with outboard location just as was identified in the previous oil flow photographs with $\alpha = 12°$. When compared with the faired inlet, the same general trend is observed; however the flow is turned more and the spanwise flow is much greater. The faired inlet clearly distorts the true inlet flow and causes greatly increased spanwise flow on the forebody at the engine-inlet plane.

To more thoroughly investigate the effects of a faired inlet, longitudinal data were obtained for both power-on and power-off conditions over an angle-of-attack range from $-3.5°$ to $12°$. These data were obtained at the approximate wheel touchdown height ($h/b = 0.08$) and are presented for comparison with baseline data in figure 19. Several differences were noted when comparing longitudinal data on the flow-through inlet configuration to the faired-inlet configuration. First, as would be expected, the faired inlet increased the drag over the flow-through inlet in the power-off condition. When comparing the lift coefficient data, there was very little difference between the power-off and the power-on condition for the faired inlet, whereas there was a substantial difference for the flow-through inlet. The largest difference in lift coefficient between the two configurations occurred for the power-on condition at negative angles of attack. In addition, at these same conditions, the largest difference in pitching moment was noted. This reveals that the high-velocity, low-pressure inlet flow associated with the flow-through inlet configuration cannot be adequately simulated by the faired inlet. This would, in turn, support the differences previously noted in the forebody surface oil flow patterns.

Afterbody Modifications

In addition to forebody inlet flow studies, exhaust flow conditions were also investigated. The dominant influence of the exhaust flow led to tests of various add-on components in the afterbody region of the configuration to determine both their fundamental effects on the longitudinal aerodynamics as well as their suitability as control devices. One area of concern was the possible power-on ground effects that may develop on a configuration with afterbody fences. The afterbody fences, as illustrated in figure 5, were mounted flush with the sides of the engine simulation system and extended the entire length of the afterbody. They were tested with the model at $\alpha = 12°$, both in and out of ground effect, and over a thrust coefficient range from 0 to 0.7.

Longitudinal aerodynamic data for the configuration with afterbody fences are presented together with the baseline data for comparison in figure 20. When the configurations are compared out of ground effect, there is little difference except for a slight loss in propulsion-system efficiency for the configuration with afterbody fences as indicated by the increase in drag. However, when the configurations are compared in ground effect (for $h/b < 0.2$), there is a much greater lift loss for the afterbody-fences configuration than for the baseline configuration. This, in turn, produces an increment in nose-up pitching moment. The afterbody fences confine all the exhaust flow to the region directly below the afterbody, and at very low ground heights the fences reduce the amount of free-stream flow that is entrained spanwise into the exhaust flow. (This is supported in the upcoming flow visualization discussion.) The afterbody fences induce a higher streamwise free-stream flow entrainment under the engine simulation system which, in turn, produces low pressures on the bottom surface of the engine pack. These low pressures produce the high lift losses noted in ground effect.

The configuration with afterbody fences was also compared with the baseline configuration in ground effect as thrust coefficient was varied. Longitudinal aerodynamic data for this comparison are presented in figure 21. These data were obtained with the model in ground effect at 2 in. above the ground ($h/b = 0.08$) and at an angle of attack of $12°$. As thrust coefficient was increased from power off to a value of 0.1, there was little difference between the two configurations; however as thrust coefficient was increased beyond 0.1, lift losses increased at a greater rate for the configuration with afterbody fences on. As noted before, the afterbody fences prohibit a lateral mixing of the exhaust flow with the free stream, thereby producing a higher velocity, lower

pressure flow beneath the model. The additional lift losses for the configuration with afterbody fences show that afterbody fences can create a substantial adverse ground effect.

Exhaust flow visualization photographs for the baseline configuration and the afterbody-fences configuration are presented together for comparison in figure 22. This flow visualization was generated by the water injection technique in combination with the laser light sheet as discussed earlier. These photographs show how the afterbody fences eliminate the spanwise spreading of the exhaust flow that occurred in ground effect on the baseline configuration. This is most evident on the right side of the model since the laser light sheet is being directed at the exhaust flow from that direction and its intensity has not yet been diminished by the density of the water mist, as is the case on the left side of the model. This flow visualization supports the discussion of the longitudinal data presented in figures 20 and 21.

Because of the extensive exhaust flow, exhaust flow deflectors were investigated as a means of longitudinal control. In the first investigation, four different exhaust flow deflectors, as identified in the sketches presented in figure 4, were tested to determine their effectiveness in separating or deflecting the exhaust flow away from the afterbody. The first two exhaust flow deflectors tested, the 0.375-in. strip and the 1-in. strip, were ineffective in separating the exhaust flow from the afterbody. Observation of exhaust flow visualization during testing showed that in both cases the exhaust flow would quickly reattach to the undersurface of the afterbody just downstream of the flow deflector. Since these two exhaust flow deflectors did not effectively separate the exhaust flow from the afterbody, no data are presented for them.

Two additional exhaust flow deflectors, the 3-in. strip and the 30° wedge strip, were investigated, and longitudinal aerodynamic data illustrating their effectiveness as the configuration was lowered into ground effect are presented in figure 23. When the 30° wedge-strip configuration is compared with the baseline configuration, it is evident that the 30° wedge strip had only a minor effect on redirecting the exhaust flow. However, when the 3-in-strip configuration is compared with the baseline configuration, a significant difference in all the longitudinal data is noted. This is not surprising since the 3-in. strip exceeds the 2.2-in. height of the engine simulation system. Observation of the exhaust flow showed that the 3-in. strip was so large that it not only separated the exhaust flow from the afterbody but it also directed the flow down, directly away from the model. Therefore, the 3-in. strip was oversized for its intended purpose of separating the exhaust flow from the afterbody.

Since the 0.375- and 1-in. strips had essentially no effect on the exhaust flow and the 30° wedge strip had a minor effect on the exhaust flow, it was evident that substantial flow deflectors, with respect to the exit height of the engine simulation system, will be required to separate the exhaust flow from the afterbody and, thus, to provide for any meaningful amount of longitudinal control.

Therefore, in the second investigation, larger exhaust flow deflectors were tested. These exhaust flow deflectors were 6-in-long wedge blocks that again spanned the width of the engine simulation system. The wedge-block angles tested were 14°, 30°, and 45°. A sketch of the size and position of the wedge blocks is presented in figure 9.

Longitudinal aerodynamic data illustrating the effects of wedge-block angle as the configuration is lowered into ground effect during power-on conditions are presented in figure 24. These data are for the wedges in the forward position just aft of the engine simulation system, as illustrated in figure 9. A comparison of the 14° wedge-block configuration with the baseline configuration shows that the 14° wedge has little effect on lift or pitching moment and a minimal effect on drag. However, the 30° wedge block produces a significant lift increase in ground effect and an increment in nose-up pitching moment out of ground effect. The 45° wedge block produces a lift increase over the entire range of h/b tested, and it also produces a similar increment in nose-up pitching moment out of ground effect as did the 30° wedge. As expected, an increase in wedge-block angle produces an increase in drag because the resultant thrust vector is deflected from the free-stream direction. Thus, with the use of a large control surface the exhaust flow can effectively be deflected for longitudinal control; however this technique is sensitive to ground effects.

To obtain better insight into the effectiveness of the larger wedges, exhaust flow visualization studies were again conducted. The exhaust flow visualization photographs presented in figure 25 illustrate the effects of the 45° wedge block in the forward position on the afterbody. The flow visualization was generated by the water injection technique in combination with the laser light sheet as explained earlier. In the side-view photograph the configuration is essentially out of ground effect, and thus it clearly shows the 45° deflection of the exhaust flow. This explains the increase in lift and nose-up pitching moment that was generated out of ground effect. In the top-view

photograph the configuration is fully in ground effect. This illustrates how a significant portion of the exhaust flow is forced to flow outboard around the wedge in the spanwise direction. This is again most evident on the right side of the model. This spanwise flow is extensive in ground effect and is not present in the side-view photograph for the model out of ground effect. The top view illustrates that in ground effect the deflected exhaust flow is confined between the wedge block and the floor, thereby producing a high-pressure region under the model and creating the increased lift. These flow visualization photographs clearly illustrate the sensitivity of the deflected exhaust flow to ground effects.

Wedge block effectiveness was further investigated by varying the longitudinal position of the wedge block on the afterbody of the configuration (fig. 9). The 45° wedge block was used in this comparison, and the longitudinal aerodynamic data are presented in figure 26. When compared with the baseline configuration, the wedge block located in the forward position produced a lift increase over the range of h/b tested and an increment in nose-up pitching moment out of ground effect as discussed earlier.

When the 45° wedge block was located in the aft position, an even larger lift increase both in and out of ground effect was noted than was the case with the wedge block in the forward position. In addition, an increment in nose-down pitching moment was produced presumably because of the resultant thrust vector acting well aft of the moment reference center.

The 45° wedge block in the aft position was also tested in combination with the afterbody fences (as illustrated in fig. 9). The longitudinal data for this configuration are also presented in figure 26. These data show that when the afterbody fences are added, the largest lift increase both in and out of ground effect is produced. This, in turn, creates the largest increment in nose-down pitching moment. Thus, the afterbody fences are very effective in improving the exhaust flow deflection generated by the wedge in the aft location.

Not only are the wedge blocks effective in generating longitudinal control but the position of this control surface and the use of afterbody fences can further enhance this control capability.

Wings and Flaps

The final area of interest in this study included the effects of adding a delta wing to the configuration as well as the effects of flap deflections during both power-on and power-off conditions.

In the first investigation a rather large 79° delta wing was tested as illustrated in figure 6. Both power-on and power-off ground effects data are presented in figure 27 to compare the baseline configuration and the 79° delta wing configuration. All aerodynamic coefficients for the 79° delta wing configuration were calculated using a 35-percent greater reference area than that used for the baseline configuration coefficients. Since thrust coefficient is also a function of reference area, it would not be appropriate to match that parameter when making power-on comparisons between the two configurations. Instead, engine weight flow rate $\dot{w}$ was matched when comparing configurations. The weight flow rate was set at 9 lb/sec for all wing-on, power-on conditions such that appropriate comparisons between the configurations could be made. (Recall that $\dot{w} = 9$ lb/sec is equivalent to $C_T = 0.4$ for the baseline configuration.)

When comparing the longitudinal aerodynamic data of figure 27 for the power-off, flow-through (F.T.) condition, it is seen that an increase in lift was generated as both the 79° delta wing configuration and the baseline configuration were lowered into ground effect. This increase in lift, however, occurred more gradually as ground height was reduced for the 79° delta wing configuration.

When the configurations were tested for power-on conditions out of ground effect, both demonstrated lift losses when compared with the corresponding power-off data. The presence of the delta wing reduced power-on ground effects in that it reduced the lift losses incurred as the baseline configuration was lowered to $h/b < 0.5$. The additional lift produced by adding a wing to the configuration appears to be offset by the lift loss generated by the power-on condition as the delta wing configuration is lowered into ground effect. This illustrates how the addition of this 79° delta wing to the configuration acts to reduce the adverse power-on ground effects.

In the second investigation, a smaller 70° delta wing, more representative of that found on a hypersonic vehicle, was tested as identified in the sketch in figure 8. In order to compare the power-on effects between the 79° delta wing and the smaller 70° delta wing, incremental lift coefficient data were obtained. These data identify the change in lift coefficient produced by going from the power-off condition to the power-on condition of $\dot{w} = 9$ lb/sec. These data are presented as the configuration is lowered into ground effect in figure 28. The data presented for the 70° delta wing were obtained with the wing in the forward position as illustrated in figure 8. These data further emphasize that the power-on lift loss

is increased as each of the configurations is lowered into ground effect. The configurations with the delta wings alone tend to have a slightly larger power-on lift loss out of ground effect than the baseline configuration; however at the lowest ground heights, the baseline configuration has a much larger power-on lift loss. When the two delta wing configurations are compared, the 70° delta wing configuration has less of a power-on lift loss in ground effect.

The final set of data presented in figure 28 illustrates the effects of adding an afterbody flap to the 70° delta wing configuration. (See fig. 8.) These data show a completely reversed trend as a positive increment in lift coefficient is identified both in and out of ground effect. This increment remains relatively constant as the configuration is lowered into ground effect with only a slight reduction appearing at the lowest ground height. Even though the afterbody flap was undeflected, it still acted to deflect the exhaust flow at an angle equivalent to the 14° afterbody ramp angle. (See fig. 8.) Thus, these data show how the presence of an afterbody flap completely eliminated the power-on lift losses that were present on the configurations without an afterbody flap.

To further investigate the effects of longitudinal wing position, the 70° delta wing was tested with wing flaps deflected 30° in both a forward and an aft position as illustrated in figure 8. Longitudinal aerodynamic data are presented for these two wing positions in figure 29. These data are presented at $\alpha = 12°$ as the configurations are lowered into ground effect for both power-off and power-on conditions. The afterbody flap was set at 0° for all cases, and the longitudinal location of the moment reference center was held fixed at 62 percent of the body length for both wing positions.

When the unpowered conditions are compared, a 30° wing flap deflection produces more lift with the wing in the forward position than in the aft position. Furthermore, a pronounced lift loss is noted in ground effect for the aft wing configuration. During powered conditions, however, slightly more lift is produced by the aft wing configuration. This is due to the wing flaps being located in a position where the expanding exhaust flow is more likely to add energy to the flow over the wing flaps.

As would be expected, the positive flap deflection creates a larger nose-down pitching moment on the aft wing configuration as compared with the forward wing configuration for both power-on and power-off conditions. An examination of the drag coefficient data reveals that the position of the wing had little effect on this component of the longitudinal data during both power-off and power-on conditions.

To look more closely at the effects of flap deflections, configurations were tested in which the wing flaps and afterbody flaps were all deflected both 30° and −30°. Longitudinal aerodynamic data are presented in figure 30(a) for these configurations with the wing in the forward position for both power-off and power-on conditions. In addition, incremental lift coefficient data illustrating the effects of flap deflections and power-on conditions are presented in figure 30(b). These incremental lift coefficients were generated by subtracting out the power-off, flaps-undeflected data.

For the −30° flap deflection and power-off condition, the expected lift loss and increase in positive pitching moment when compared with the 0° flap deflection are shown. The opposite trends result, as expected, for the 30° flap deflections. However, during these power-off conditions the lift increments created by both positive and negative flap deflections are slightly reduced as the configuration is lowered to the minimum ground height as illustrated in figure 30(b).

When power is added to the configuration, the lift and pitching-moment increments are increased out of ground effect as compared with the power-off case. However, as the configuration is lowered into ground effect, these increments are further increased, in contrast to the reduced increments seen for the power-off condition. The increased magnitude of the power-on lift increments in ground effect are also seen in the incremental data presented in figure 30(b). Thus, it is seen that the effects of flap deflections are influenced by power and are sensitive to ground effects.

A final set of data was obtained in which the afterbody flap was deflected 30° with the wing flaps held fixed at 0°. Longitudinal aerodynamic data for both power-on and power-off conditions are presented in figure 31(a). Data for both the afterbody flap alone deflected 30° and for all flaps deflected 30° are presented to provide insight into the independent effects of the flap deflections. Furthermore, incremental lift coefficient data illustrating the effects of the flap deflections and power-on conditions are presented in figure 31(b). These incremental lift coefficients were again generated by subtracting out the power-off, flaps-undeflected data.

The longitudinal data of figure 31(a) reveal that the power-on condition significantly increases the lift and nose-down pitching moment created by the 30° afterbody flap deflection, thus showing that the

afterbody flap is much more directly affected by the exhaust flow than the wing flaps.

When comparing the incremental lift coefficient data of figure 31(b), the difference between the wing-flaps-deflected data and the wing-flaps-undeflected data is the same for the power-on condition as it is for the power-off condition out of ground effect. This identifies the power-on condition as having very little effect on the deflected wing flaps. It is also noted that the power-on lift increment for the afterbody flap alone deflected increases in ground effect, just as it did for the configurations with all flaps deflected.

Summary of Results

The results of the investigations of a powered, generic hypersonic configuration tested in and out of ground effect in the NASA Langley 14- by 22-Foot Subsonic Tunnel are summarized as follows:

1. Power-on lift losses in ground effect will become greater with increasing thrust, but they will be significantly reduced as angle of attack is increased to the order of the afterbody ramp angle.

2. Spanwise flow on the undersurface of the forebody in the vicinity of the engine inlets is most evident at positive angles of attack in ground effect. However, inlet fences can eliminate this spanwise flow. In addition, a faired inlet will not accurately simulate flowing inlet conditions in ground effect.

3. The use of afterbody fences produces increased lift losses in ground effect with power on.

4. Afterbody wedge-block tests demonstrate that an afterbody control surface can effectively deflect the exhaust flow for longitudinal control; however this technique is sensitive to ground effects.

5. The addition of a delta wing to the configuration acts to reduce the power-on lift loss in ground effect, whereas the addition of an afterbody flap generates a power-on lift increase. However, the effects of both afterbody flap and wing flap deflections are influenced by power and can be sensitive to ground effects.

NASA Langley Research Center
Hampton, VA 23665-5225
March 28, 1991

References

1. Gatlin, Gregory M.: *Low-Speed, High-Lift Aerodynamic Characteristics of Slender, Hypersonic Accelerator-Type Configurations.* NASA TP-2945, 1989.

2. Hahne, David E.; Riebe, Gregory D.; Riley, Donald R.; and Pegg, Robert J.: *Exploratory Wind-Tunnel Investigation of the Low-Speed Aerodynamic Characteristics of a Conical Aerospace Plane Concept.* NASA TP-2860, 1989.

3. Gatlin, Gregory M.: *Low-Speed Aerodynamic Characteristics of a Powered Nasp-Like Configuration in Ground Effect.* SAE Tech. Paper Ser. 892312, Sept. 1989.

4. Gentry, Garl L., Jr.; Quinto, P. Frank; Gatlin, Gregory M.; and Applin, Zachary T.: *The Langley 14- by 22-Foot Subsonic Tunnel: Description, Flow Characteristics, and Guide for Users.* NASA TP-3008, 1990.

Table I. Basic Model Geometry

Body length, in.	112.89
Body span, b, in.	24.00
Mean geometric chord of body, $\bar{c}$, in.	91.10
Model planform reference area, S, ft^2:	
Baseline configuration	15.183
Rectangular forebody configuration	18.815
79° delta wing configuration	20.433
70° delta wing configuration	18.933
70° delta wing configuration with afterbody flap	19.933

Table II. Test Configurations and Conditions

[AB: afterbody; FB: forebody; F.T.: flow through]

(a) Baseline aerodynamics

Run	Figure	Parameter varied	C_T	q_∞, psf	α, deg	Configuration
1	11, 27	h/b	0	40	12	Baseline
2	11, 23	↓	.2	40	↓	↓
3	11	↓	.4	40	↓	↓
4	11	↓	.6	26	↓	↓
5	11	↓	.8	20	↓	↓
6	12	↓	.4	40	8	↓
7	12	↓	↓	↓	10	↓
8	12, 20, 27, 28	↓	↓	↓	12	↓
9	12	↓	↓	↓	13	↓
10	12	↓	↓	↓	14	↓

(b) Inlet flow conditions

Run	Figure	Parameter varied	$\dot{w}$, lb/sec	q_∞, psf	α, deg	Configuration
11	16	h/b	F.T.	30	12	Baseline
12	16, 24, 26	↓	9	↓	↓	Baseline
13	16, 17	↓	F.T.	↓	↓	Rectang. FB
14	16, 17	↓	9	↓	↓	Rectang. FB
15	17	↓	F.T.	↓	↓	Rectang. FB with inlet fences
16	17	↓	9	↓	↓	Rectang. FB with inlet fences
17	19	α	F.T.	↓	Varied	Baseline; $h/b = 0.08$
18	↓	↓	5	↓	↓	Baseline; $h/b = 0.08$
19	↓	↓	0	↓	↓	Faired inlet; $h/b = 0.08$
20	↓	↓	5	↓	↓	Faired inlet; $h/b = 0.08$

Table II. Continued

(c) Afterbody modifications

Run	Figure	Parameter varied	C_T	q_∞, psf	α, deg	Configuration
21	20	h/b	0.4	40	12	AB fences on
22	21	C_T	Varied	20		Baseline; $h/b = 0.08$
23	21	C_T	Varied	20		AB fences on; $h/b = 0.08$
24	23	h/b	.2	40		3-in. AB strip
25	23		.2	40		30° AB wedge strip
26	24		.4	30		14° AB wedge block
27	24					30° AB wedge block
28	24, 26					45° AB wedge block
29	26					45° AB wedge block (AFT)
30	26	↓	↓	↓	↓	45° AB wedge block (AFT) with AB fences

(d) Wing and flaps

Run	Figure	Parameter varied	$\dot{w}$, lb/sec	q_∞, psf	α, deg	Configuration
31	27	h/b	F.T.	40	12	79° delta wing on
32	27, 28		9	40		79° delta wing on
33	28		F.T.	30		70° delta wing (FWD) with rectang. FB
34	28		9			70° delta wing (FWD) with rectang. FB
35	28, 29, 30, 31		F.T.			70° delta wing (FWD) with undeflected AB flap
36	28		9			70° delta wing (FWD) with undeflected AB flap
37	29	↓	F.T.	↓	↓	70° delta wing (FWD); $\delta_F = 30°$; $\delta_{ABF} = 0°$

Table II. Concluded

(d) Concluded

Run	Figure	Parameter varied	$\dot{w}$, lb/sec	q_∞, psf	α, deg	Configuration
38	29	h/b	9	30	12	70° delta wing (FWD); $\delta_F = 30°$; $\delta_{ABF} = 0°$
39	↓	↓	F.T.	↓	↓	70° delta wing (AFT); $\delta_F = 30°$; $\delta_{ABF} = 0°$
40	↓	↓	9	↓	↓	70° delta wing (AFT); $\delta_F = 30°$; $\delta_{ABF} = 0°$
41	30	↓	F.T.	↓	↓	70° delta wing (FWD); $\delta_F = -30°$; $\delta_{ABF} = -30°$
42	30	↓	9	↓	↓	70° delta wing (FWD); $\delta_F = -30°$; $\delta_{ABF} = -30°$
43	30, 31	↓	F.T.	↓	↓	70° delta wing (FWD); $\delta_F = 30°$; $\delta_{ABF} = 30°$
44	30, 31	↓	9	↓	↓	70° delta wing (FWD); $\delta_F = 30°$; $\delta_{ABF} = 30°$
45	31	↓	F.T.	↓	↓	70° delta wing (FWD); $\delta_F = 0°$; $\delta_{ABF} = 30°$
46	31	↓	9	↓	↓	70° delta wing (FWD); $\delta_F = 0°$; $\delta_{ABF} = 30°$

Table III. Longitudinal Aerodynamic Force and Moment Data

RUN = 1

H/B	CL	CD	CM	CT	ALPHA	Q
.0467	.2781	.1015	.0882	.0000	12.01	40.00
.0891	.2169	.0956	.0895	.0000	12.08	40.08
.1679	.1642	.0892	.0880	.0000	12.04	40.02
.3333	.1468	.0812	.0832	.0000	12.01	40.26
.5001	.1475	.0758	.0795	.0000	11.97	40.22
.7509	.1421	.0761	.0775	.0000	12.02	40.02
1.0018	.1492	.0732	.0775	.0000	12.09	40.24
1.5001	.1431	.0705	.0753	.0000	12.08	40.07
2.0022	.1367	.0721	.0734	.0000	12.06	40.25
2.5000	.1374	.0645	.0726	.0000	12.05	40.39
2.9310	.1308	.0651	.0722	.0000	12.05	40.07

RUN = 2

H/B	CL	CD	CM	CT	ALPHA	Q
.0465	.1140	-.0352	.1022	.1962	12.22	40.39
.0893	.0800	-.0591	.1002	.2025	11.95	40.27
.1669	.0876	-.0730	.0954	.2029	12.00	40.17
.3341	.0998	-.0827	.0893	.2027	11.96	40.16
.5000	.0977	-.0847	.0865	.2024	11.95	40.18
.7501	.0951	-.0808	.0838	.2013	12.00	40.34
1.0004	.0990	-.0848	.0833	.2019	11.99	40.19
1.5004	.1047	-.0907	.0814	.2022	11.99	40.12
2.0004	.1013	-.0923	.0804	.2028	11.97	39.93
2.5000	.1085	-.0987	.0785	.2033	11.94	39.92
2.8940	.0996	-.0982	.0781	.2037	11.93	39.77

RUN = 3

H/B	CL	CD	CM	CT	ALPHA	Q
.0469	.0390	-.2038	.1144	.3949	12.06	40.50
.0886	.0418	-.2289	.1099	.3990	12.04	40.11
.1665	.0583	-.2298	.1046	.3935	12.01	40.30
.3334	.0820	-.2413	.0980	.3947	12.00	40.34
.4999	.0889	-.2399	.0955	.3899	11.98	40.44
.7499	.0879	-.2428	.0945	.3960	11.97	40.49
1.0001	.0875	-.2483	.0945	.3987	11.96	40.19
1.5001	.1030	-.2562	.0920	.3977	11.96	40.38
2.0002	.0949	-.2558	.0917	.3989	11.95	40.27
2.5003	.0831	-.2508	.0872	.3986	11.91	40.26
2.8665	.0906	-.2614	.0878	.4032	11.90	39.84

Table III. Continued

RUN = 4

H/B	CL	CD	CM	CT	ALPHA	Q
.0421	-.0261	-.4109	.1170	.5912	11.89	26.33
.0837	.0024	-.4409	.1110	.5969	11.89	26.17
.1710	.0435	-.4586	.1074	.5965	11.90	26.25
.3333	.0673	-.4631	.1049	.5937	11.90	26.40
.5000	.0788	-.4690	.1021	.5992	11.89	26.19
.7501	.0958	-.4831	.1009	.6056	11.89	25.90
1.0008	.0991	-.4863	.1001	.6097	11.88	25.73
1.5001	.0958	-.4840	.0986	.6070	11.87	25.84
2.0001	.0866	-.4833	.0974	.6069	11.85	25.89
2.5003	.0843	-.4825	.0939	.6027	11.83	26.13
2.8723	.0828	-.4797	.0934	.6041	11.83	26.08

RUN = 5

H/B	CL	CD	CM	CT	ALPHA	Q
.0418	-.0752	-.5823	.1205	.7853	11.77	20.03
.0836	-.0336	-.6200	.1142	.7841	11.77	19.98
.1673	.0144	-.6306	.1119	.7781	11.79	20.11
.3353	.0640	-.6467	.1091	.7813	11.79	20.06
.5003	.0766	-.6408	.1056	.7735	11.79	20.30
.7501	.0842	-.6592	.1059	.7908	11.78	19.88
1.0000	.0932	-.6586	.1044	.7888	11.78	19.90
1.5002	.1050	-.6569	.1025	.7854	11.78	19.95
2.0008	.0988	-.6507	.1004	.7760	11.76	20.07
2.5008	.0864	-.6531	.0988	.7820	11.75	19.89
2.8732	.0852	-.6579	.0968	.7829	11.73	19.91

RUN = 6

H/B	CL	CD	CM	CT	ALPHA	Q
.0587	-.1482	-.2246	.0885	.3997	7.94	40.51
.0964	-.0995	-.2433	.0836	.4028	7.95	40.22
.1672	-.0642	-.2498	.0798	.4030	7.95	40.25
.3334	-.0227	-.2657	.0740	.4010	7.96	40.46
.5004	-.0155	-.2661	.0715	.4023	7.96	40.32
.7500	.0017	-.2722	.0696	.4004	7.97	40.53
1.0004	.0074	-.2756	.0696	.4023	7.97	40.38
1.5003	.0024	-.2713	.0682	.4006	7.96	40.54
2.0001	.0070	-.2770	.0668	.4043	7.94	40.21
2.3086	.0008	-.2758	.0652	.4045	7.92	40.20

Table III. Continued

RUN = 7

H/B	CL	CD	CM	CT	ALPHA	Q
.0503	-.0682	-.2168	.1043	.4009	10.04	39.97
.0962	-.0285	-.2364	.0948	.3976	10.02	40.32
.1667	-.0004	-.2440	.0921	.3986	10.01	40.25
.3336	.0316	-.2592	.0856	.3999	10.01	40.09
.5004	.0351	-.2572	.0841	.3991	9.99	40.18
.7502	.0425	-.2600	.0817	.4010	9.97	40.00
1.0003	.0451	-.2610	.0812	.3983	9.98	40.26
1.4999	.0488	-.2647	.0803	.3999	9.97	40.12
2.0004	.0489	-.2653	.0776	.4003	9.95	40.13
2.5003	.0448	-.2666	.0758	.4006	9.91	40.12
2.5899	.0445	-.2638	.0748	.3994	9.91	40.24

RUN = 8

H/B	CL	CD	CM	CT	ALPHA	Q
.0101	.0383	-.2120	.1167	.4014	12.12	39.49
.0206	.0437	-.2243	.1152	.4008	12.12	39.60
.0410	.0349	-.2325	.1118	.4000	12.09	39.63
.0837	.0543	-.2406	.1081	.3936	12.10	40.29
.1670	.0735	-.2561	.1056	.3980	12.10	39.85
.3335	.0908	-.2603	.1015	.3997	12.07	39.66
.5017	.0941	-.2624	.0983	.4004	12.05	39.57
.7521	.1008	-.2657	.0969	.3995	12.05	39.65
1.0001	.1029	-.2622	.0940	.3975	12.03	39.73
1.5000	.1009	-.2707	.0939	.4062	12.04	39.87

RUN = 9

H/B	CL	CD	CM	CT	ALPHA	Q
.0106	.1571	-.1942	.1186	.3911	13.33	40.63
.0209	.1278	-.2060	.1183	.3943	13.31	40.37
.0424	.0963	-.2157	.1161	.3947	13.28	40.36
.0866	.1006	-.2385	.1149	.3946	13.29	40.39
.1668	.1077	-.2471	.1128	.3957	13.28	40.29
.3332	.1192	-.2507	.1087	.3961	13.25	40.35
.5015	.1308	-.2532	.1056	.3960	13.24	40.39
.7534	.1277	-.2561	.1038	.3976	13.23	40.26
1.0006	.1327	-.2634	.1034	.4039	13.22	40.00
1.4998	.1336	-.2698	.1035	.4013	13.22	39.87

Table III. Continued

RUN = 10

H/B	CL	CD	CM	CT	ALPHA	Q
.0103	.2249	-.2035	.1152	.3989	14.28	40.18
.0207	.2126	-.2093	.1163	.4005	14.27	40.05
.0419	.1776	-.2196	.1146	.3990	14.25	40.22
.0837	.1594	-.2345	.1153	.3988	14.26	40.24
.1665	.1468	-.2449	.1162	.4010	14.25	40.01
.3337	.1478	-.2487	.1141	.4030	14.23	39.84
.5000	.1542	-.2492	.1108	.4037	14.21	39.80
.7510	.1476	-.2473	.1078	.4004	14.19	40.10
1.0002	.1596	-.2577	.1089	.4045	14.20	39.70
1.5001	.1472	-.2529	.1062	.3996	14.18	40.12

RUN = 11

H/B	CL	CD	CM	W	ALPHA	Q
.0214	.2874	.0835	.0740	2.94	12.11	29.70
.0430	.2536	.0749	.0754	3.11	12.13	30.94
.0841	.1929	.0715	.0749	3.16	12.06	29.70
.1670	.1512	.0639	.0739	3.22	12.05	29.81
.3335	.1404	.0553	.0701	3.23	12.03	30.26
.5014	.1339	.0562	.0673	3.23	12.01	30.26
.7501	.1251	.0556	.0652	3.21	11.99	30.04
1.0037	.1233	.0534	.0638	3.21	11.99	30.26
1.5011	.1306	.0474	.0644	3.20	11.98	29.92
2.0006	.1334	.0423	.0642	3.21	12.00	30.15

RUN = 12

H/B	CL	CD	CM	W	ALPHA	Q
.0224	.0232	-.2451	.0965	8.99	12.34	30.38
.0440	.0108	-.2825	.0944	8.97	12.35	30.26
.0852	.0223	-.3118	.0898	8.92	12.09	30.26
.1682	.0338	-.3222	.0854	8.93	12.05	29.24
.3354	.0756	-.3183	.0814	8.84	12.06	30.15
.5034	.0841	-.3123	.0799	8.81	12.07	30.49
.7515	.0915	-.3107	.0773	8.76	12.04	30.38
1.0017	.0970	-.3284	.0771	8.89	12.04	30.26
1.5015	.0839	-.3201	.0759	8.89	12.04	30.49
2.0005	.0882	-.3214	.0745	8.86	12.02	30.26

Table III. Continued

RUN = 13

H/B	CL	CD	CM	W	ALPHA	Q
.0231	.3046	.0766	.1276	2.97	12.08	29.92
.0419	.2759	.0704	.1263	3.05	12.05	30.04
.0866	.2289	.0632	.1254	3.21	12.04	30.49
.1674	.1930	.0556	.1188	3.23	11.95	29.81
.3354	.1634	.0490	.1147	3.26	11.90	29.70
.5037	.1574	.0456	.1123	3.25	12.07	29.81
.7525	.1442	.0439	.1086	3.24	12.03	29.92
1.0013	.1508	.0397	.1052	3.23	12.00	29.81
1.4996	.1391	.0381	.1052	3.24	12.00	30.15
2.0027	.1338	.0423	.1036	3.24	11.99	29.92

RUN = 14

H/B	CL	CD	CM	W	ALPHA	Q
.0244	.1161	-.1907	.1402	8.99	12.26	30.15
.0425	.0844	-.2147	.1381	8.98	12.23	30.15
.0850	.0894	-.2270	.1322	8.97	12.22	30.49
.1694	.0942	-.2432	.1306	8.96	12.21	30.26
.3374	.1018	-.2483	.1245	8.96	12.18	30.38
.5019	.0972	-.2538	.1220	8.94	12.14	30.26
.7529	.0988	-.2531	.1180	8.94	12.12	30.38
1.0018	.0951	-.2553	.1153	8.93	12.10	30.04
1.5003	.0919	-.2535	.1147	8.94	12.10	30.38
2.0016	.0900	-.2557	.1131	8.95	12.10	30.38

RUN = 15

H/B	CL	CD	CM	W	ALPHA	Q
.0202	.2793	.0665	.1196	2.93	12.18	30.26
.0446	.2560	.0648	.1206	2.99	12.18	30.15
.0843	.2128	.0538	.1201	3.13	12.15	30.15
.1658	.1539	.0490	.1172	3.20	12.08	29.58
.3352	.1357	.0404	.1111	3.21	12.03	30.04
.5038	.1282	.0404	.1067	3.22	12.00	30.04
.7533	.1270	.0400	.1027	3.20	11.97	29.92
1.0035	.1348	.0361	.0999	3.19	11.95	29.81
1.5011	.1233	.0342	.0999	3.19	11.95	29.92
2.0000	.1237	.0270	.1009	3.18	11.94	29.92

Table III. Continued

RUN = 16

H/B	CL	CD	CM	W	ALPHA	Q
.0222	.0793	-.1853	.1328	8.97	12.10	30.15
.0457	.0429	-.2114	.1327	9.00	12.10	30.04
.0841	.0472	-.2256	.1289	9.00	12.10	30.49
.1678	.0775	-.2408	.1233	8.99	12.08	30.71
.3316	.0856	-.2526	.1169	9.00	12.02	30.04
.5018	.0897	-.2540	.1141	9.00	11.99	30.15
.7528	.0935	-.2580	.1107	8.98	11.97	30.26
.9996	.0947	-.2576	.1071	9.01	11.95	30.26
1.4996	.0912	-.2588	.1081	9.09	11.96	30.60
2.0009	.0962	-.2594	.1065	9.01	11.97	30.60

RUN = 17

H/B	CL	CD	CM	W	ALPHA	Q
.0639	-.2182	.0663	.0130	3.68	-3.96	30.26
.0842	-.1463	.0585	.0216	3.50	-2.07	30.04
.0875	-.0832	.0504	.0310	3.42	.00	30.49
.0865	-.0306	.0442	.0386	3.34	2.04	30.83
.0846	.0103	.0463	.0487	3.27	4.11	30.38
.0823	.1039	.0519	.0623	3.25	8.09	30.60
.0837	.2178	.0686	.0761	3.16	12.10	30.38

RUN = 18

H/B	CL	CD	CM	W	ALPHA	Q
.0894	-.3205	.0483	.0120	5.04	-3.52	30.38
.0854	-.2609	.0229	.0185	5.01	-2.05	30.15
.0826	-.2086	.0122	.0278	5.05	-.05	30.04
.0874	-.1428	.0037	.0360	5.06	2.04	30.04
.0855	-.0969	-.0057	.0452	5.06	4.01	30.15
.0852	.0090	-.0031	.0639	5.04	8.06	30.15
.0872	.1415	.0090	.0801	5.06	12.08	30.04

Table III. Continued

RUN = 19

H/B	CL	CD	CM	W	ALPHA	Q
.0863	-.2015	.0858	.0294	.00	-3.56	29.81
.0792	-.1467	.0747	.0342	.00	-1.94	29.92
.0868	-.1091	.0634	.0415	.00	.10	30.04
.0866	-.0639	.0601	.0475	.00	2.14	30.15
.0841	-.0170	.0550	.0571	.00	4.15	29.92
.0865	.0566	.0613	.0676	.00	8.15	30.26
.0832	.1840	.0825	.0804	.00	12.10	29.81

RUN = 20

H/B	CL	CD	CM	W	ALPHA	Q
.0820	-.2041	.0033	.0254	4.99	-3.47	29.92
.0849	-.1555	-.0110	.0295	4.95	-2.03	30.38
.0861	-.1201	-.0103	.0367	4.98	.00	30.15
.0851	-.0720	-.0195	.0448	4.97	2.08	30.15
.0838	-.0379	-.0169	.0529	4.97	4.08	30.04
.0852	.0557	-.0142	.0698	4.98	8.05	30.15
.0844	.1749	.0015	.0852	4.99	12.10	29.92

RUN = 21

H/B	CL	CD	CM	CT	ALPHA	Q
.0106	-.1830	-.1487	.1284	.3711	12.04	40.02
.0210	-.1228	-.1840	.1244	.3714	12.07	40.04
.0423	-.0684	-.2147	.1217	.3741	12.10	39.69
.0839	.0099	-.2360	.1136	.3706	12.12	40.08
.1667	.0672	-.2377	.1034	.3671	12.09	40.51
.3329	.0910	-.2464	.0962	.3686	12.06	40.34
.5011	.0970	-.2484	.0934	.3710	12.04	40.10
.7511	.1020	-.2531	.0936	.3704	12.04	40.12
1.0000	.1023	-.2553	.0920	.3711	12.04	40.08
1.5007	.1023	-.2538	.0902	.3697	12.02	40.15

Table III. Continued

RUN = 22

H/B	CL	CD	CM	CT	ALPHA	Q
.0800	.2399	.0860	.0892	.0204	12.69	20.22
.0800	.1462	.0133	.0946	.0914	12.73	20.27
.0800	.1231	-.0958	.0959	.2030	12.80	20.14
.0800	.1067	-.1853	.0995	.3186	12.86	20.51
.0800	.0987	-.2577	.1045	.4126	12.90	20.40
.0800	.0844	-.3193	.1079	.4935	12.92	20.13
.0800	.0539	-.4238	.1136	.6095	12.98	20.16
.0800	.0442	-.5161	.1193	.7100	13.04	20.25
.0800	.0382	-.5754	.1233	.7926	13.08	20.31

RUN = 23

H/B	CL	CD	CM	CT	ALPHA	Q
.0800	.2444	.0887	.0860	.0146	12.65	20.29
.0800	.1380	-.0126	.0894	.0993	12.69	20.44
.0800	.0937	-.1068	.0946	.2007	12.75	20.12
.0800	.0572	-.1835	.1000	.3029	12.80	20.16
.0800	.0319	-.2732	.1078	.4074	12.86	20.20
.0800	-.0165	-.3498	.1161	.5062	12.89	20.05
.0800	-.0861	-.4497	.1256	.6063	12.95	20.20
.0800	-.1148	-.5266	.1358	.6989	13.01	20.15

RUN = 24

H/B	CL	CD	CM	CT	ALPHA	Q
.0421	.4383	.1218	.0976	.1976	12.05	40.00
.0839	.2800	.0977	.1156	.1972	12.10	40.02
.1664	.2574	.0852	.1229	.1984	12.15	39.76
.3330	.2247	.0891	.1405	.1986	12.24	39.63
.5002	.2132	.0756	.1437	.1984	12.27	39.68
.7511	.1993	.0738	.1410	.1982	12.25	39.70
1.0014	.1959	.0687	.1391	.1977	12.24	39.78
1.5001	.1897	.0686	.1374	.1959	12.22	40.10

Table III. Continued

RUN = 25

H/B	CL	CD	CM	CT	ALPHA	Q
.0104	.1223	-.0505	.1259	.2086	12.14	39.96
.0211	.0990	-.0535	.1267	.2079	12.13	40.04
.0416	.0666	-.0577	.1249	.2054	12.11	40.46
.0836	.0505	-.0699	.1190	.2081	12.05	39.87
.1668	.0751	-.0803	.1047	.2065	11.97	39.99
.3333	.0897	-.0842	.0948	.2040	11.91	40.30
.5009	.1027	-.0913	.0915	.2036	11.90	40.19
.7504	.0940	-.0870	.0874	.2020	11.86	40.13
1.0020	.1043	-.0919	.0879	.2015	11.87	40.07
1.5007	.0955	-.0881	.0854	.2016	11.84	40.02

RUN = 26

H/B	CL	CD	CM	W	ALPHA	Q
.0218	.1192	-.2073	.1173	9.13	12.09	30.26
.0435	.0205	-.2583	.1087	9.12	12.07	30.26
.0867	.0076	-.2686	.0988	9.14	11.99	30.38
.1268	.0277	-.2743	.0901	9.11	12.02	30.60
.1693	.0323	-.2703	.0868	9.08	12.00	30.38
.2506	.0672	-.2840	.0848	9.03	12.07	30.15
.3349	.0743	-.2839	.0825	9.00	12.07	30.15
.5009	.0779	-.2839	.0789	8.98	12.03	30.15
.7519	.0965	-.2941	.0777	8.98	12.05	30.15
1.0015	.0861	-.2878	.0755	8.96	12.02	30.26
1.5021	.0876	-.2857	.0735	8.96	12.01	30.38
2.0034	.0975	-.2957	.0753	8.97	12.02	30.15

RUN = 27

H/B	CL	CD	CM	W	ALPHA	Q
.0653	.6302	.0535	.0712	8.98	11.97	30.15
.0834	.4020	-.0492	.0942	8.87	12.08	30.38
.1268	.1689	-.1797	.1153	8.99	12.07	30.94
.1687	.1545	-.2051	.1182	9.05	12.06	30.38
.2510	.0864	-.2046	.1211	8.99	12.06	30.38
.3346	.0833	-.2105	.1176	8.99	12.04	30.38
.5027	.0728	-.2157	.1110	9.01	11.99	30.38
.7512	.1048	-.2205	.1044	9.00	12.05	30.26
1.0002	.0943	-.2236	.1046	9.00	12.05	30.49
1.5001	.0973	-.2242	.1024	9.02	12.03	30.26
2.0021	.0798	-.2192	.1032	9.01	12.03	30.26

Table III. Continued

RUN = 28

H/B	CL	CD	CM	W	ALPHA	Q
.1702	.5118	.0698	.0744	9.06	12.03	29.92
.2506	.2944	-.0830	.1027	8.96	12.08	30.38
.3349	.2658	-.0899	.1145	8.94	12.14	30.26
.5003	.2227	-.0982	.1147	9.02	11.98	30.26
.7508	.2040	-.1031	.1102	9.00	12.02	30.26
.9997	.2004	-.1028	.1068	8.99	11.99	30.26
1.4998	.1940	-.1075	.1090	9.00	11.97	30.15
2.0005	.2077	-.1177	.1075	9.00	11.99	30.15

RUN = 29

H/B	CL	CD	CM	W	ALPHA	Q
.1661	.5427	.0453	-.0001	9.02	12.05	30.04
.2504	.3132	-.0845	.0548	9.00	11.99	30.26
.3355	.2954	-.1179	.0662	9.00	12.09	30.49
.5014	.2830	-.1234	.0673	9.01	12.10	30.38
.7502	.2557	-.1115	.0658	9.01	12.08	30.38
.9997	.2490	-.1182	.0687	9.01	12.10	30.60
1.5002	.2419	-.1232	.0715	9.00	12.09	30.26
2.0000	.2319	-.1078	.0663	8.99	12.06	30.38

RUN = 30

H/B	CL	CD	CM	W	ALPHA	Q
.1700	.5859	.0469	-.0071	9.00	12.05	29.70
.2517	.3983	-.0994	.0370	8.91	12.02	30.38
.3340	.3834	-.1246	.0471	9.00	12.10	30.04
.5005	.3790	-.1195	.0443	9.00	12.09	30.38
.7534	.3647	-.1193	.0442	8.99	12.09	30.15
1.0035	.3645	-.1234	.0436	9.00	12.08	30.04
1.5010	.3684	-.1284	.0420	9.01	12.08	30.15
2.0027	.3494	-.1222	.0444	8.99	12.08	29.81

Table III. Continued

RUN = 31

H/B	CL	CD	CM	W	ALPHA	Q
.0103	.4620	.1256	.0766	2.86	11.93	40.18
.0209	.4520	.1265	.0765	2.89	11.92	40.08
.0417	.4369	.1281	.0734	3.01	11.88	39.82
.0835	.4309	.1286	.0667	3.13	11.82	39.79
.1666	.4216	.1202	.0608	3.16	11.78	40.09
.3333	.3795	.1225	.0571	3.19	11.72	40.02
.5005	.3769	.1089	.0567	3.22	11.72	40.12
.7512	.3642	.1073	.0554	3.22	11.70	40.17
1.0010	.3502	.1068	.0549	3.20	11.69	40.12
1.5001	.3424	.1051	.0531	3.20	11.66	39.96

RUN = 32

H/B	CL	CD	CM	W	ALPHA	Q
.0107	.2893	-.1939	.0885	9.09	12.14	40.16
.0209	.2898	-.2018	.0871	9.07	12.12	39.88
.0419	.3017	-.2062	.0898	9.00	12.16	40.29
.0841	.2940	-.2098	.0875	8.98	12.14	40.43
.1666	.2843	-.2131	.0891	8.97	12.15	40.01
.3334	.3065	-.2203	.0839	8.95	12.14	40.43
.5005	.3047	-.2231	.0839	8.97	12.12	40.20
.7511	.2951	-.2241	.0806	8.97	12.09	39.97
1.0017	.3028	-.2289	.0797	8.98	12.09	40.10
1.5019	.2917	-.2289	.0788	9.00	12.08	40.21
2.0007	.2926	-.2312	.0773	8.99	12.06	40.22

RUN = 33

H/B	CL	CD	CM	W	ALPHA	Q
.0336	.2693	.0664	.1038	2.92	12.13	30.26
.0433	.2377	.0623	.1028	3.01	12.09	30.15
.0859	.2169	.0620	.0941	3.13	11.99	30.15
.1702	.2197	.0645	.0800	3.16	11.86	29.92
.3356	.2163	.0596	.0738	3.19	11.93	30.26
.5036	.2139	.0560	.0723	3.22	11.92	30.71
.7524	.2035	.0558	.0707	3.22	11.98	30.83
1.0012	.2048	.0547	.0687	3.20	11.97	30.60
1.4588	.1999	.0563	.0667	3.20	12.00	30.49
2.0023	.1948	.0549	.0659	3.19	11.98	30.26

Table III. Continued

RUN = 34

H/B	CL	CD	CM	W	ALPHA	Q
.0216	.1758	-.1292	.1158	9.07	12.31	29.92
.0425	.1157	-.1537	.1032	9.00	12.17	29.81
.0836	.1322	-.1793	.0917	8.98	12.11	30.26
.1673	.1395	-.1886	.0895	8.97	12.09	30.26
.3340	.1584	-.1908	.0822	8.95	12.04	30.15
.5027	.1577	-.1951	.0819	8.97	12.02	30.15
.7523	.1559	-.1937	.0784	8.97	11.98	30.15
1.0019	.1547	-.2005	.0785	8.98	11.98	29.70
1.5005	.1549	-.1985	.0757	9.00	11.96	29.92
2.0011	.1523	-.1954	.0740	8.99	11.94	30.04

RUN = 35

H/B	CL	CD	CM	W	ALPHA	Q
.0235	.3132	.0816	.0367	2.94	12.08	30.04
.0451	.2760	.0809	.0349	3.08	12.04	30.38
.0841	.2751	.0866	.0288	3.13	11.98	30.04
.1677	.2816	.0880	.0185	3.17	11.89	29.92
.3363	.2681	.0832	.0162	3.21	11.85	30.04
.5042	.2631	.0794	.0155	3.21	11.84	30.04
.7535	.2549	.0832	.0140	3.21	11.83	29.92
1.0001	.2572	.0816	.0139	3.21	11.84	29.92
1.5013	.2455	.0849	.0141	3.21	12.05	30.15
2.0040	.2550	.0786	.0146	3.20	12.05	29.81

RUN = 36

H/B	CL	CD	CM	W	ALPHA	Q
.0202	.3580	-.1107	-.0365	8.98	11.99	29.36
.0450	.3552	-.1271	-.0358	8.97	12.07	30.71
.0839	.3483	-.1440	-.0310	8.96	12.12	30.38
.1681	.3390	-.1557	-.0207	8.95	12.23	30.26
.3336	.3395	-.1750	-.0121	8.93	12.10	30.26
.5014	.3219	-.1665	-.0125	8.91	12.08	30.15
.7506	.3217	-.1694	-.0130	8.91	12.08	30.04
1.0027	.3200	-.1734	-.0126	8.93	12.09	29.81
1.5018	.3144	-.1762	-.0118	8.92	12.09	29.92
1.9995	.3157	-.1759	-.0128	8.92	12.08	29.70

Table III. Continued

RUN = 37

H/B	CL	CD	CM	W	ALPHA	Q
.0244	.3855	.1251	.0072	2.98	12.04	30.15
.0418	.3833	.1261	.0034	3.04	11.99	30.38
.0843	.3854	.1359	-.0046	3.08	11.92	30.26
.1700	.4116	.1376	-.0111	3.08	12.12	30.15
.3335	.3994	.1437	-.0173	3.12	12.05	30.15
.5005	.4060	.1415	-.0187	3.13	12.03	29.92
.7523	.3829	.1466	-.0189	3.15	12.02	30.04
1.0042	.3794	.1466	-.0191	3.15	12.01	30.26
1.5031	.3702	.1439	-.0180	3.16	12.02	30.38
2.0033	.3677	.1451	-.0180	3.16	12.02	29.92

RUN = 38

H/B	CL	CD	CM	W	ALPHA	Q
.0215	.4728	-.0867	-.0725	9.02	12.09	30.15
.0424	.4913	-.1037	-.0694	9.03	12.12	30.15
.0855	.4771	-.1045	-.0650	9.03	12.16	30.38
.1696	.4687	-.1115	-.0558	9.03	12.23	30.15
.3365	.4717	-.1140	-.0513	9.04	12.08	30.38
.4998	.4691	-.1183	-.0515	9.03	12.09	30.04
.7495	.4590	-.1143	-.0511	9.03	12.09	30.04
1.0006	.4544	-.1181	-.0486	9.03	12.10	30.15
1.5029	.4513	-.1242	-.0481	9.01	12.10	29.92
2.0002	.4565	-.1234	-.0487	9.01	12.10	30.04

RUN = 39

H/B	CL	CD	CM	W	ALPHA	Q
.0622	.3088	.1082	.0068	3.09	12.11	30.15
.0873	.3177	.1127	-.0018	3.12	12.03	30.15
.1270	.3307	.1202	-.0109	3.12	11.96	29.81
.1671	.3446	.1219	-.0154	3.13	12.06	29.81
.2534	.3473	.1273	-.0236	3.14	11.99	29.92
.3335	.3522	.1291	-.0280	3.14	11.95	29.92
.5028	.3526	.1348	-.0322	3.15	12.07	30.04
.7539	.3518	.1355	-.0345	3.15	12.05	29.92
1.0016	.3538	.1352	-.0364	3.15	12.03	29.92
1.5018	.3607	.1323	-.0368	3.15	12.03	29.81
2.0041	.3490	.1385	-.0378	3.15	12.01	29.92

Table III. Continued

RUN = 40

H/B	CL	CD	CM	W	ALPHA	Q
.0418	.4728	-.0749	-.1106	9.00	11.91	30.38
.0842	.4896	-.0928	-.1083	8.96	11.96	30.26
.1287	.4928	-.1070	-.0998	8.96	12.05	30.38
.1683	.4807	-.1022	-.0964	8.94	12.06	30.38
.2524	.4758	-.1092	-.0898	8.96	12.13	30.38
.3338	.4869	-.1125	-.0892	8.95	12.14	30.26
.5006	.4856	-.1078	-.0891	8.95	12.13	30.15
.7529	.4778	-.1058	-.0888	8.96	12.13	30.49
1.0039	.4857	-.1103	-.0882	8.95	12.15	30.15
1.5009	.4743	-.1086	-.0873	8.94	12.16	30.15
2.0035	.4818	-.1088	-.0872	8.96	12.15	30.38

RUN = 41

H/B	CL	CD	CM	W	ALPHA	Q
.0211	.0705	.0546	.1138	2.89	12.19	29.81
.0448	.0252	.0516	.1065	3.12	12.09	29.92
.0845	.0124	.0507	.1000	3.21	12.03	29.81
.1271	.0058	.0501	.0953	3.26	12.00	30.15
.1675	.0071	.0497	.0913	3.26	11.96	30.04
.2540	.0026	.0527	.0887	3.25	12.09	29.92
.3342	.0032	.0485	.0878	3.25	12.09	29.92
.5036	.0067	.0449	.0845	3.24	12.06	30.04
.7526	.0085	.0441	.0819	3.22	12.04	29.70
1.0001	.0014	.0424	.0817	3.22	12.03	29.81
1.5035	.0065	.0406	.0802	3.21	12.02	29.81
2.0042	.0024	.0431	.0799	3.23	12.02	30.04

RUN = 42

H/B	CL	CD	CM	W	ALPHA	Q
.0420	-.2377	-.1838	.1588	9.03	12.14	30.49
.0842	-.2131	-.2221	.1494	9.03	12.01	30.38
.1268	-.1932	-.2256	.1439	9.03	11.99	30.49
.1680	-.1842	-.2256	.1405	9.03	11.97	30.49
.2504	-.1575	-.2383	.1387	9.03	12.08	30.04
.3335	-.1420	-.2385	.1345	9.02	12.05	30.04
.5038	-.1329	-.2364	.1304	9.01	12.04	30.26
.7502	-.1253	-.2374	.1267	9.02	12.00	30.26
1.0001	-.1238	-.2353	.1244	9.02	11.98	30.15
1.5008	-.1201	-.2352	.1226	9.01	12.05	30.15
2.0040	-.1045	-.2417	.1228	9.01	12.08	30.15

Table III. Continued

RUN = 43

H/B	CL	CD	CM	W	ALPHA	Q
.0625	.4331	.1450	-.0087	2.94	12.07	30.26
.0841	.4260	.1515	-.0150	2.97	12.00	30.49
.1266	.4440	.1507	-.0201	2.99	11.96	30.38
.1678	.4463	.1513	-.0220	3.00	12.09	30.49
.2505	.4410	.1621	-.0292	3.01	12.02	30.49
.3333	.4440	.1621	-.0314	3.03	12.00	30.38
.5003	.4550	.1576	-.0330	3.04	12.00	30.26
.7501	.4512	.1666	-.0384	3.05	11.94	30.26
1.0039	.4491	.1659	-.0387	3.06	12.09	30.38
1.5019	.4444	.1659	-.0383	3.07	12.09	30.38
2.0013	.4369	.1669	-.0393	3.06	12.07	30.38

RUN = 44

H/B	CL	CD	CM	W	ALPHA	Q
.0625	1.0410	.1460	-.2771	9.03	12.11	30.60
.0839	1.0305	.1112	-.2593	9.03	12.28	30.26
.1287	.8976	.0622	-.2102	9.02	12.08	30.38
.1693	.8276	.0470	-.1857	9.00	12.03	30.38
.2511	.7867	.0235	-.1652	9.02	12.04	30.26
.3344	.8062	.0159	-.1650	9.03	12.06	30.15
.5010	.8217	.0329	-.1745	9.03	11.97	30.38
.7515	.8111	.0342	-.1734	9.01	11.97	30.26
1.0000	.8100	.0358	-.1735	9.01	11.98	30.15
1.5011	.7973	.0370	-.1722	9.02	11.98	30.04
2.0029	.8022	.0363	-.1715	9.03	11.99	30.26

RUN = 45

H/B	CL	CD	CM	W	ALPHA	Q
.0648	.3670	.1087	.0124	2.91	12.10	30.04
.0836	.3520	.1043	.0129	2.97	12.10	29.92
.1247	.3423	.1080	.0072	3.01	12.04	29.81
.1671	.3422	.1097	.0028	3.00	12.00	29.36
.2514	.3396	.1064	-.0005	3.05	11.96	29.92
.3326	.3326	.1124	-.0039	3.06	11.96	30.15
.4998	.3435	.1097	-.0075	3.07	11.99	29.81
.7511	.3488	.1122	-.0120	3.08	11.96	29.70
.9997	.3472	.1130	-.0131	3.09	11.94	29.81
1.5001	.3550	.1070	-.0140	3.08	12.00	29.92
2.0006	.3401	.1131	-.0139	3.09	11.98	29.92

Table III. Concluded

RUN = 46

H/B	CL	CD	CM	W	ALPHA	Q
.0642	.9610	.0905	-.2525	8.97	11.95	30.15
.0850	.9052	.0538	-.2301	9.00	12.11	30.38
.1254	.8195	.0130	-.1903	8.99	12.16	30.26
.1696	.7652	-.0142	-.1617	8.95	12.13	30.49
.2515	.7024	-.0223	-.1416	9.04	12.11	30.26
.3334	.7158	-.0291	-.1402	9.01	12.13	29.92
.5000	.7248	-.0111	-.1507	9.01	12.03	30.15
.7542	.7245	-.0171	-.1484	9.00	12.05	30.04
1.0006	.7144	-.0100	-.1484	8.99	12.04	29.92
1.5005	.7080	-.0147	-.1456	9.00	12.07	29.81
2.0025	.7036	-.0130	-.1441	9.00	12.07	30.04

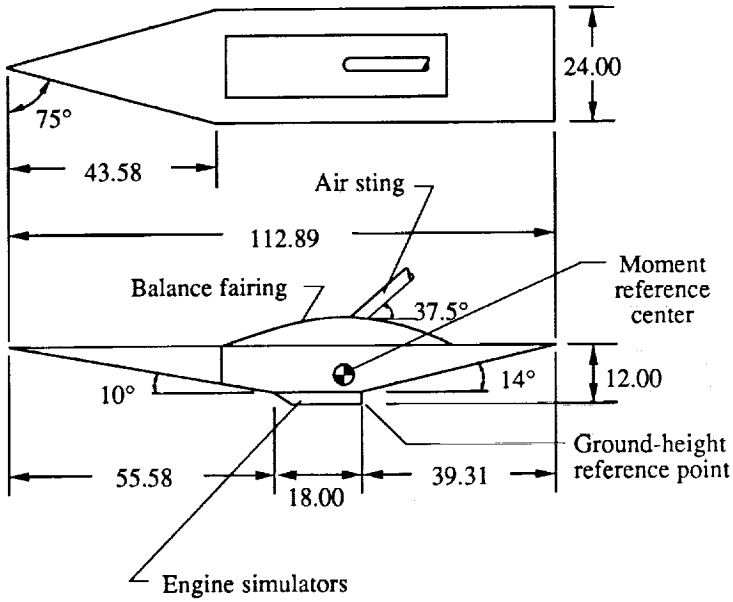

Figure 1. Sketch of generic hypersonic ground effects model (baseline configuration). All linear dimensions are given in inches.

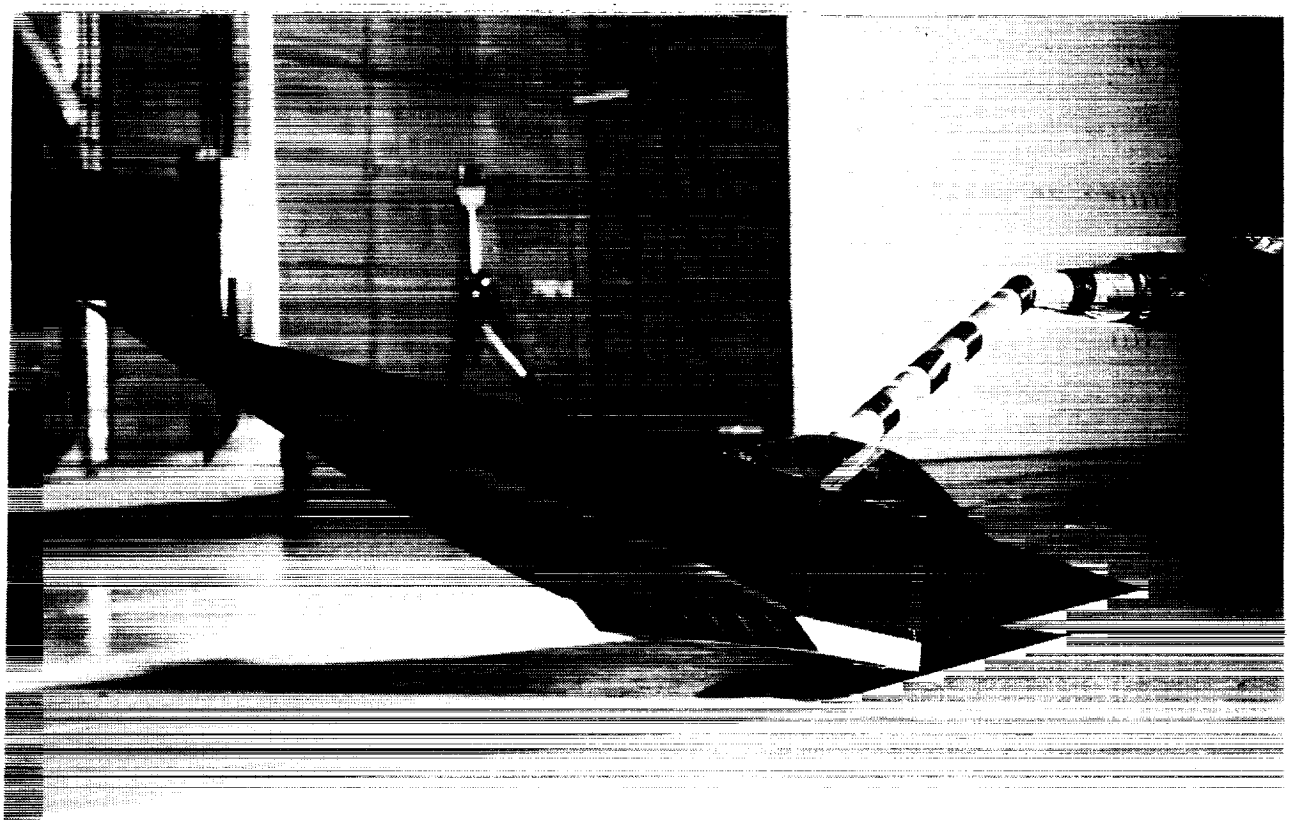

L-88-13521

Figure 2. Installation of generic hypersonic ground effects model in the Langley 14- by 22-Foot Subsonic Tunnel.

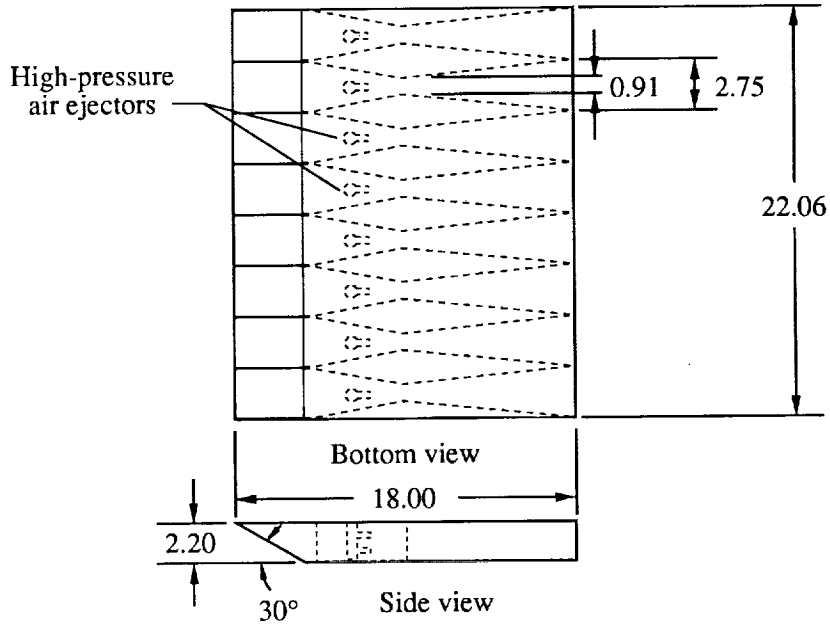

Figure 3. Sketch of engine simulation system of generic hypersonic ground effects model. All linear dimensions are given in inches.

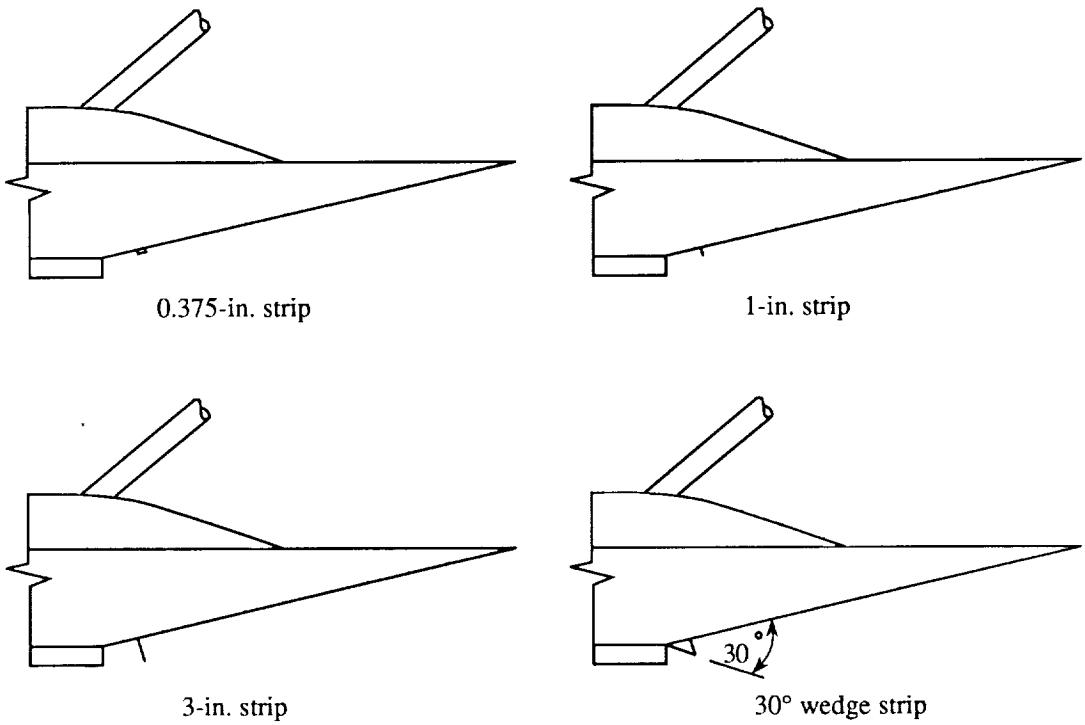

Figure 4. Sketches illustrating size and position of exhaust flow deflectors.

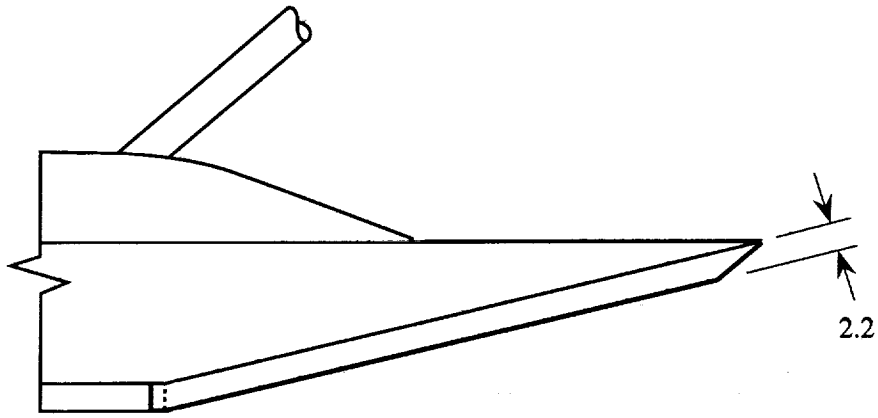

Figure 5. Sketch illustrating size and position of afterbody fences. Linear dimensions are given in inches.

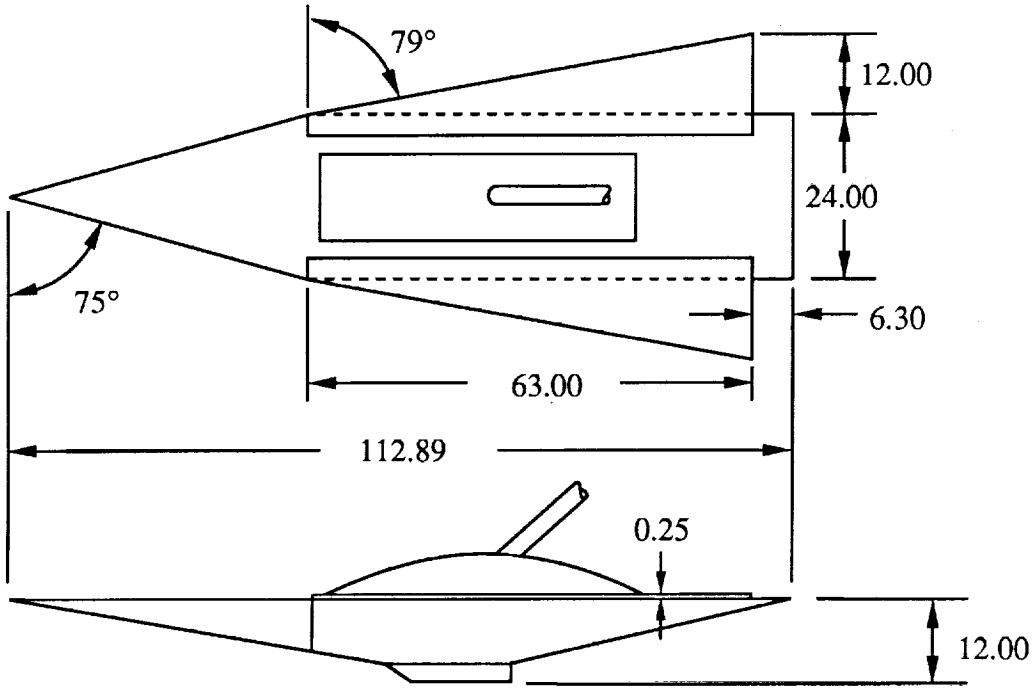

Figure 6. Sketch of 79° delta wing configuration. Linear dimensions are given in inches.

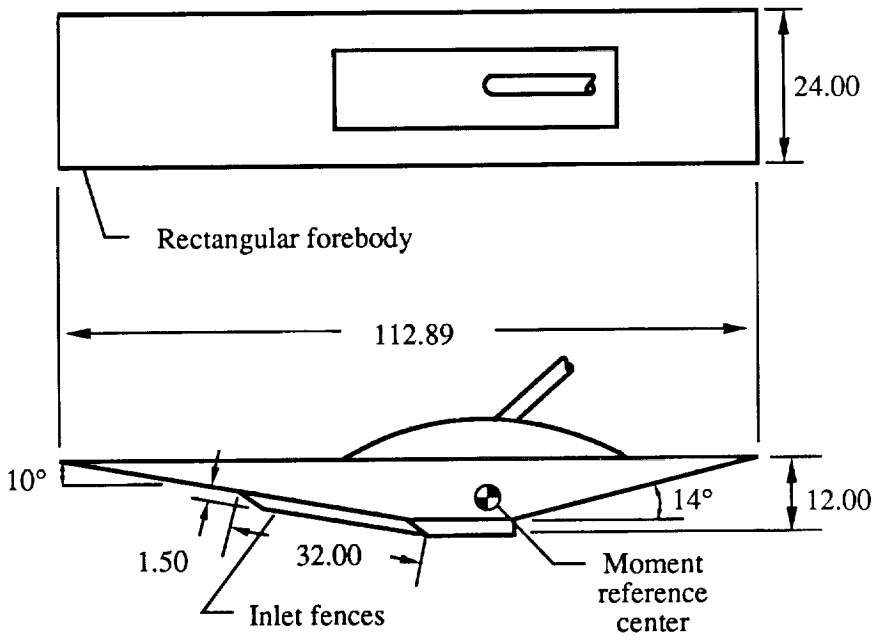

Figure 7. Sketch of model with rectangular forebody and inlet fences. All linear dimensions are given in inches.

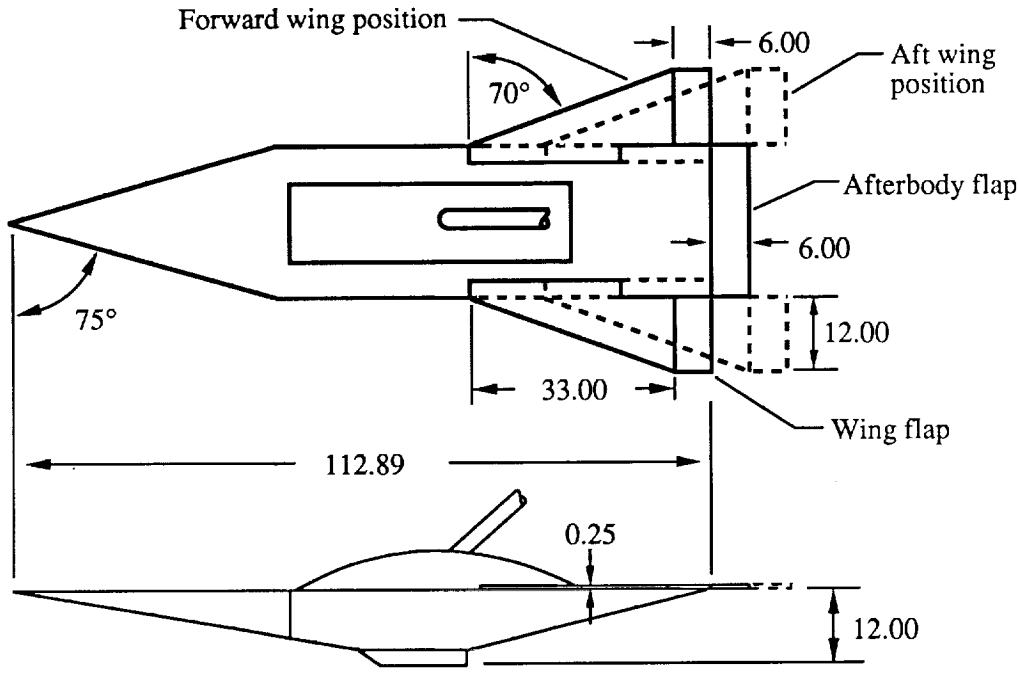

Figure 8. Sketch of 70° delta wing and flap locations. All linear dimensions are given in inches.

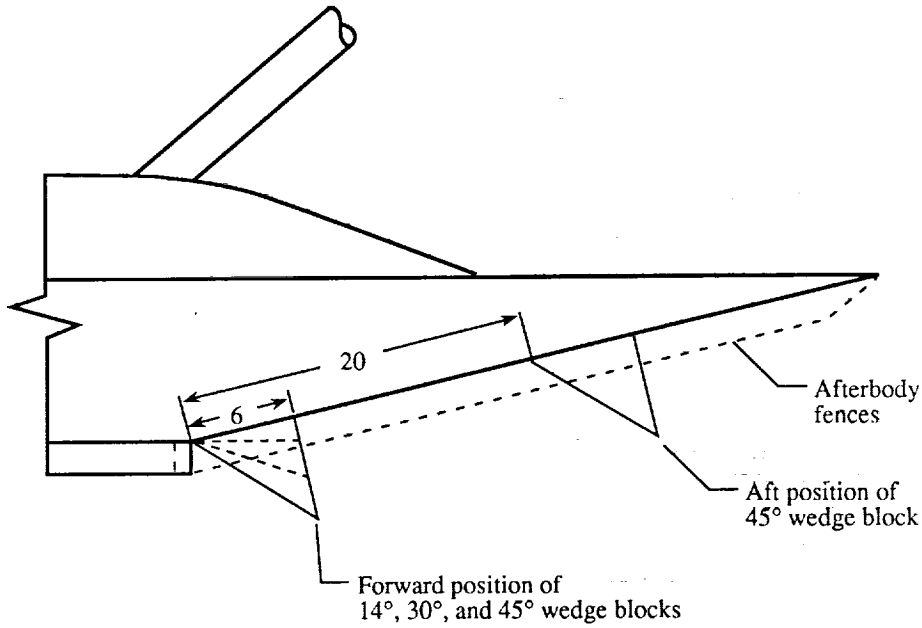

Figure 9. Locations of afterbody wedge blocks and fences. All linear dimensions are given in inches.

Figure 10. Exhaust flow visualization on generic hypersonic ground effects model. $\alpha = 12°$; $C_T = 0.4$; $h/b = 0.06$; $q_\infty = 30$ psf.

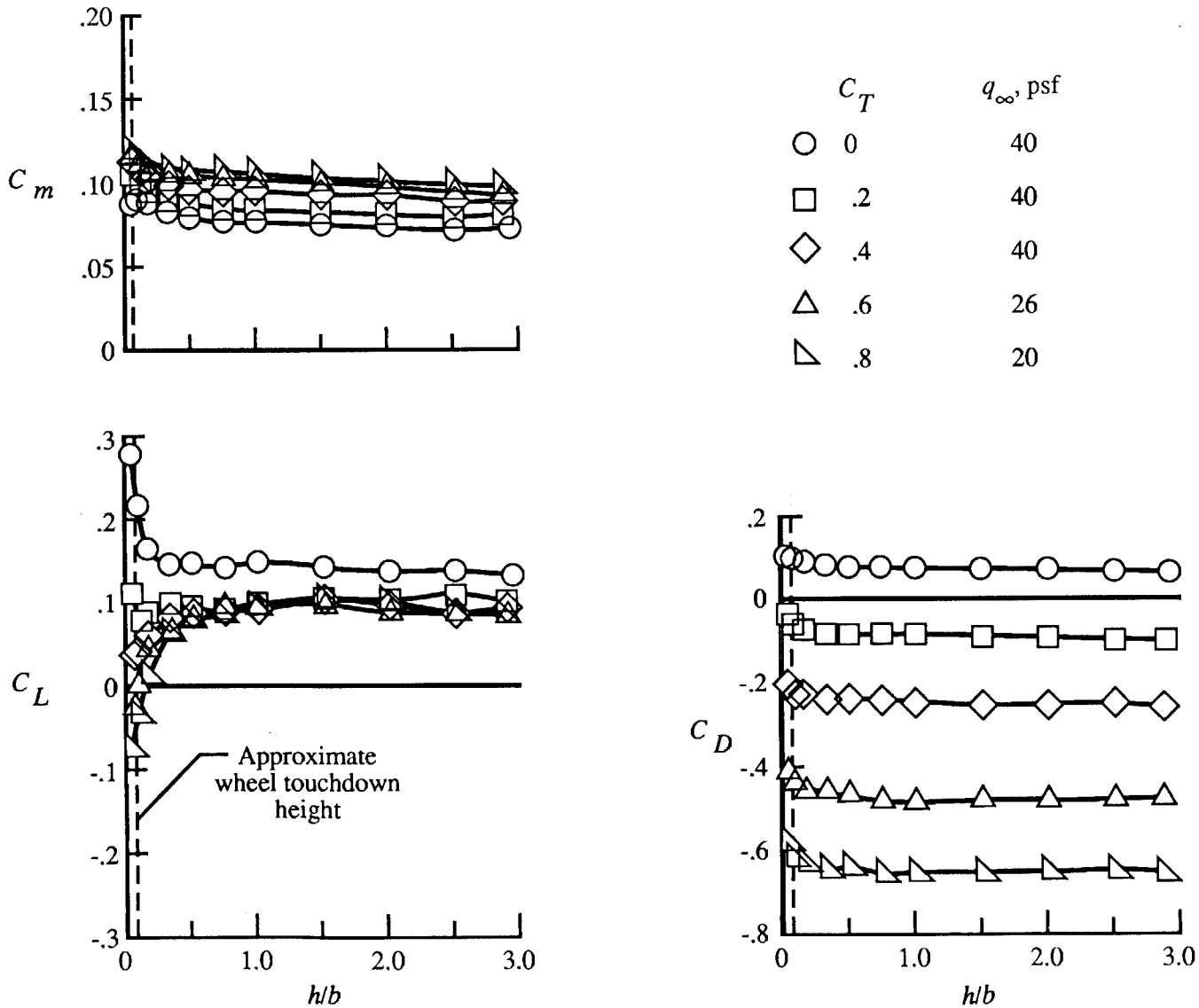

Figure 11. Ground effects data for variations in thrust coefficient. Baseline configuration; $\alpha = 12°$.

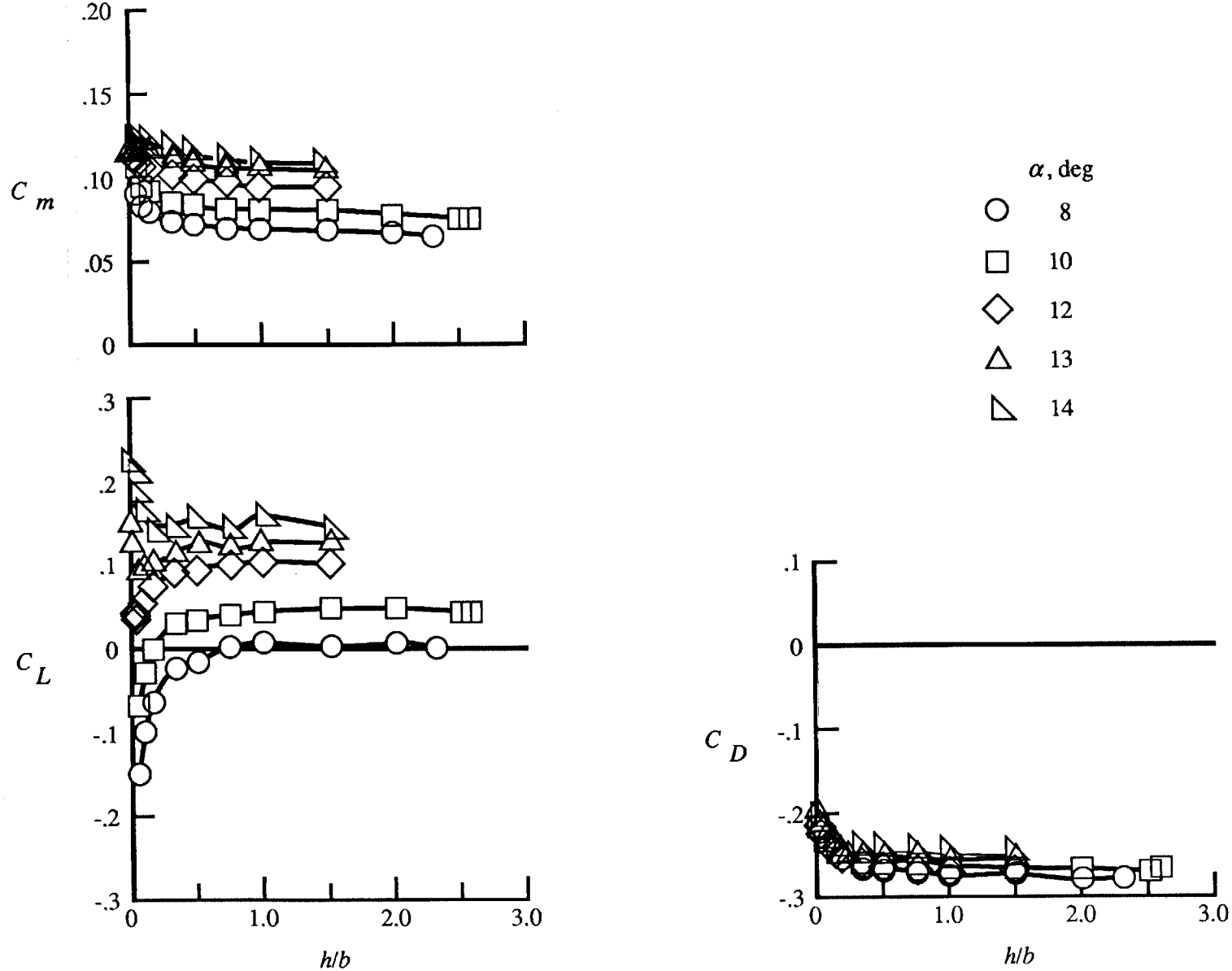

Figure 12. Power-on ground effects data for variations in angle of attack. Baseline configuration; $C_T = 0.04$; $q_\infty = 40$ psf.

Figure 13. Evidence of spanwise component of inlet flow on midsection of model with forebody removed.

ORIGINAL PAGE
BLACK AND WHITE PHOTOGRAPH

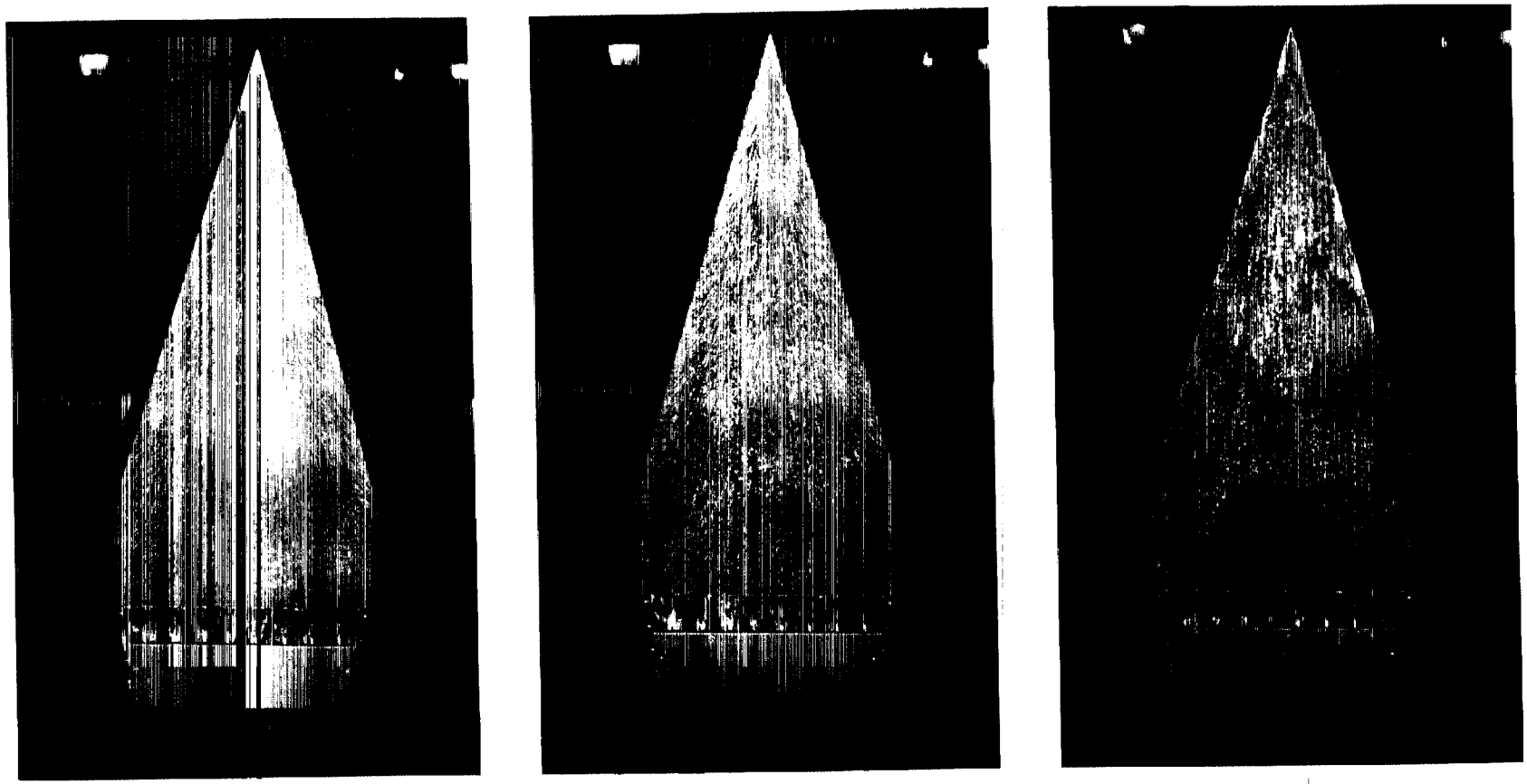

(a) $\alpha = 12°$; $h/b = 2.30$.

(b) $\alpha = 12°$; $h/b = 0.08$.

(c) $\alpha = -3.5°$; $h/b = 0.08$.

Figure 14. Surface oil flow visualization illustrating ground effects on inlet flow. $C_T = 0.4$; $q_\infty = 30$ psf.

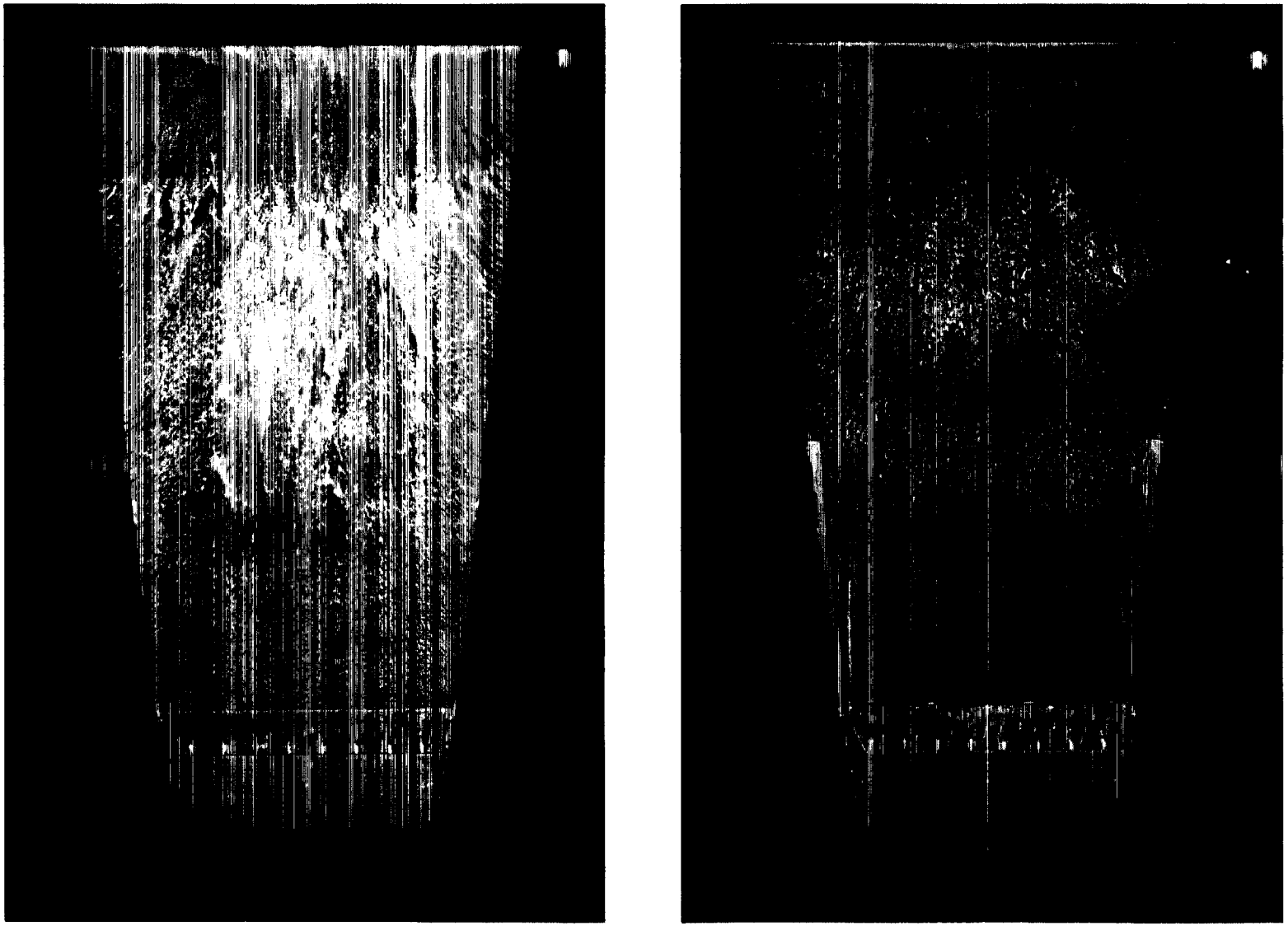

(a) Inlet fences off.

(b) Inlet fences on.

Figure 15. Surface oil flow visualization illustrating effects of inlet fences on inlet flow. $\alpha = 12°$; $C_T = 0.4$; $h/b = 0.08$; $q_\infty = 30$ psf.

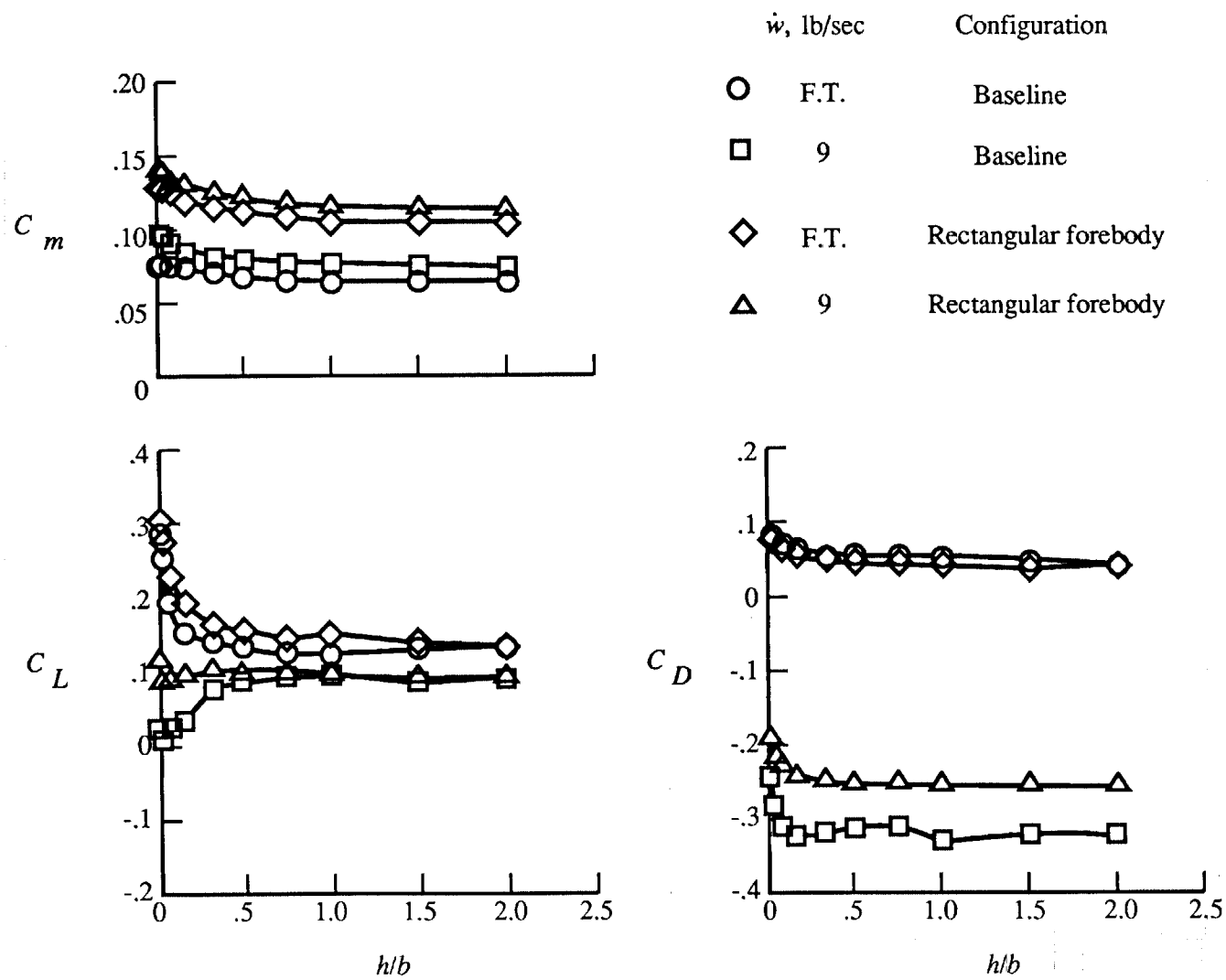

Figure 16. Ground effects data illustrating effects of rectangular forebody. $\alpha = 12°$; $q_\infty = 30$ psf.

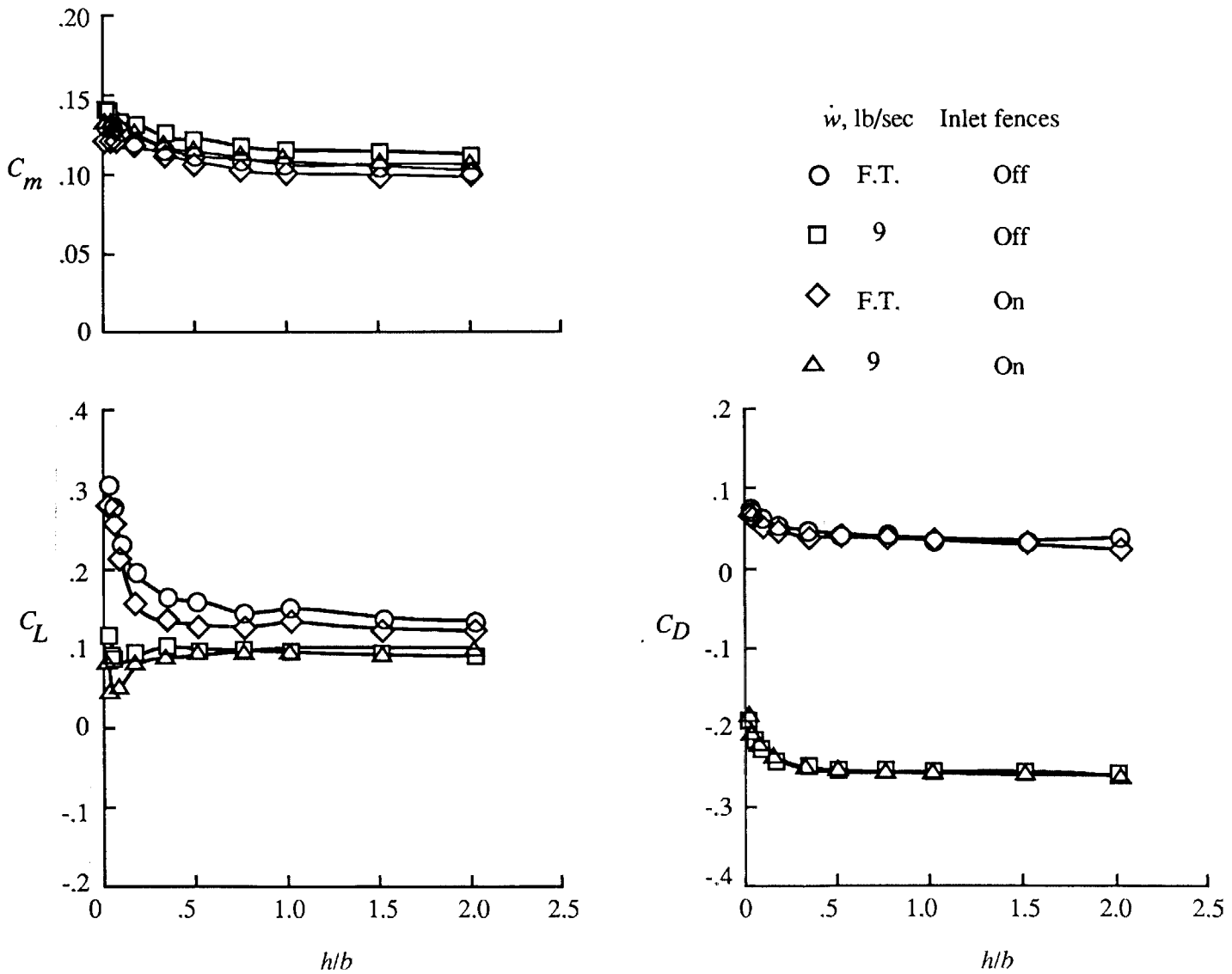

Figure 17. Ground effects data with rectangular forebody illustrating effects of inlet fences. $\alpha = 12°$; $q_\infty = 30$ psf.

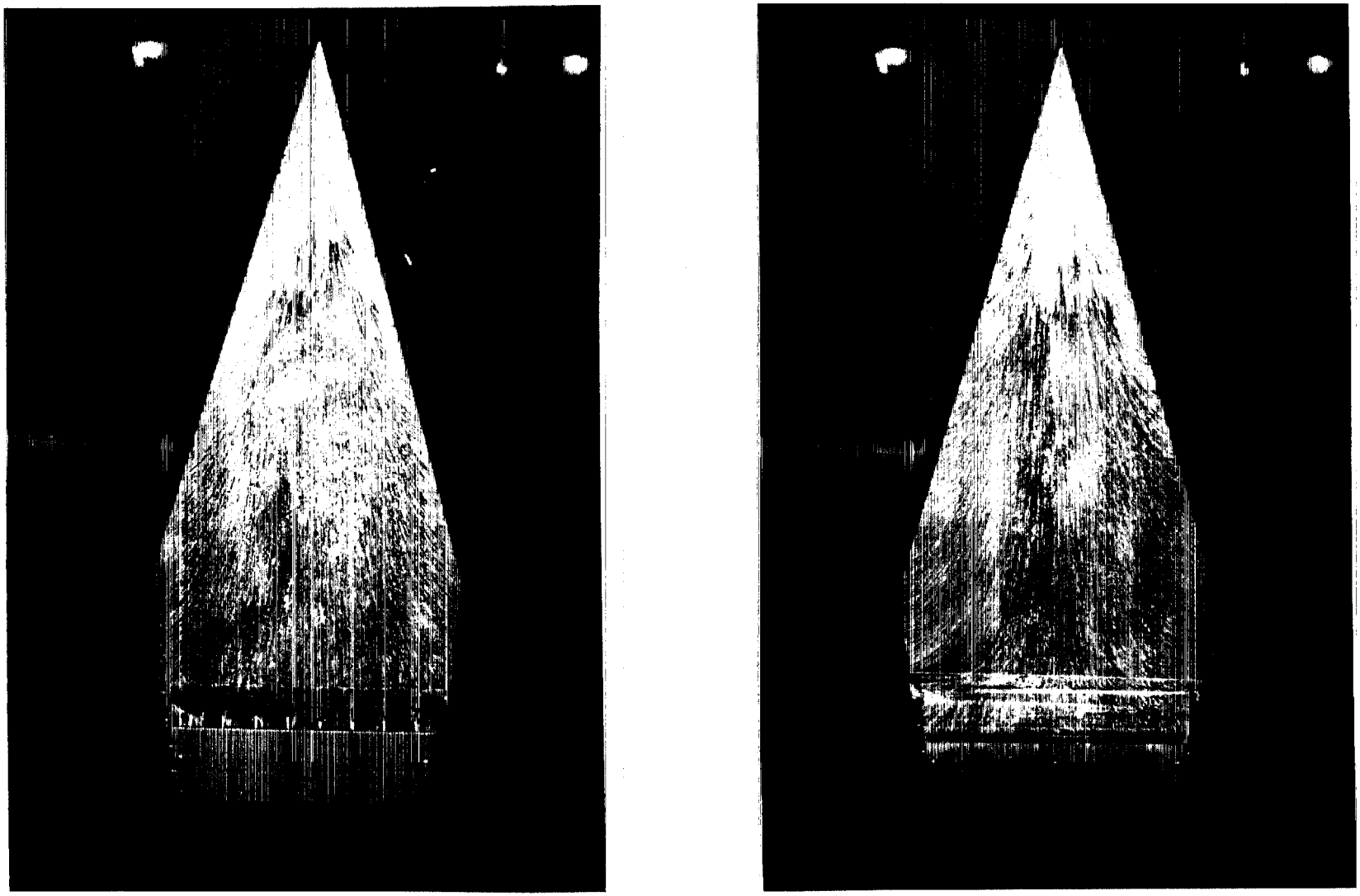

(a) Flow-through inlet.

(b) Faired inlet.

Figure 18. Surface oil flow visualization illustrating effects of faired inlet. $\alpha = 12°$; $h/b = 0.08$; $\dot{w} = 5$ lb/sec; $q_\infty = 30$ psf.

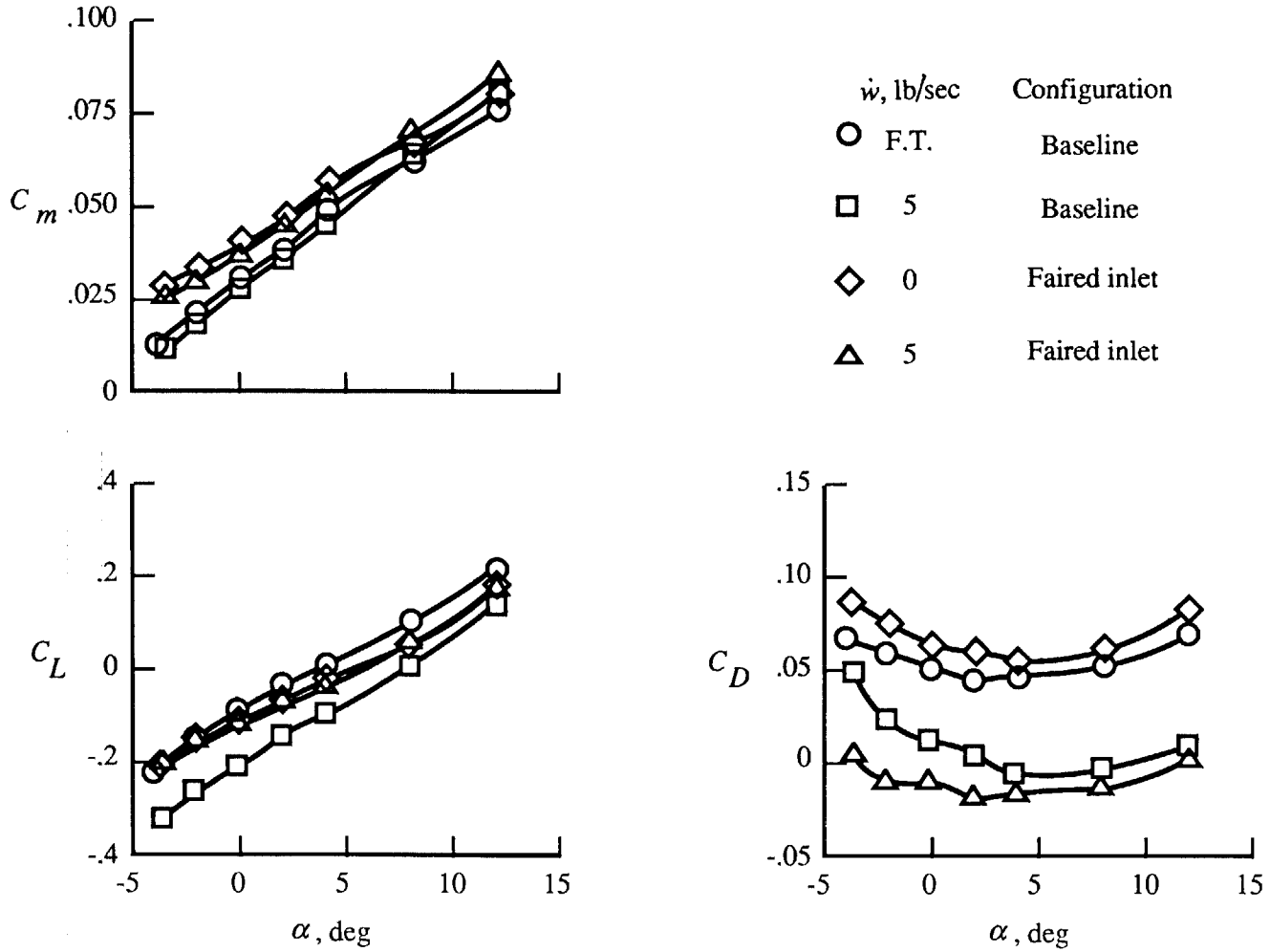

Figure 19. Longitudinal data illustrating effects of faired inlet. $h/b = 0.08$; $q_\infty = 30$ psf.

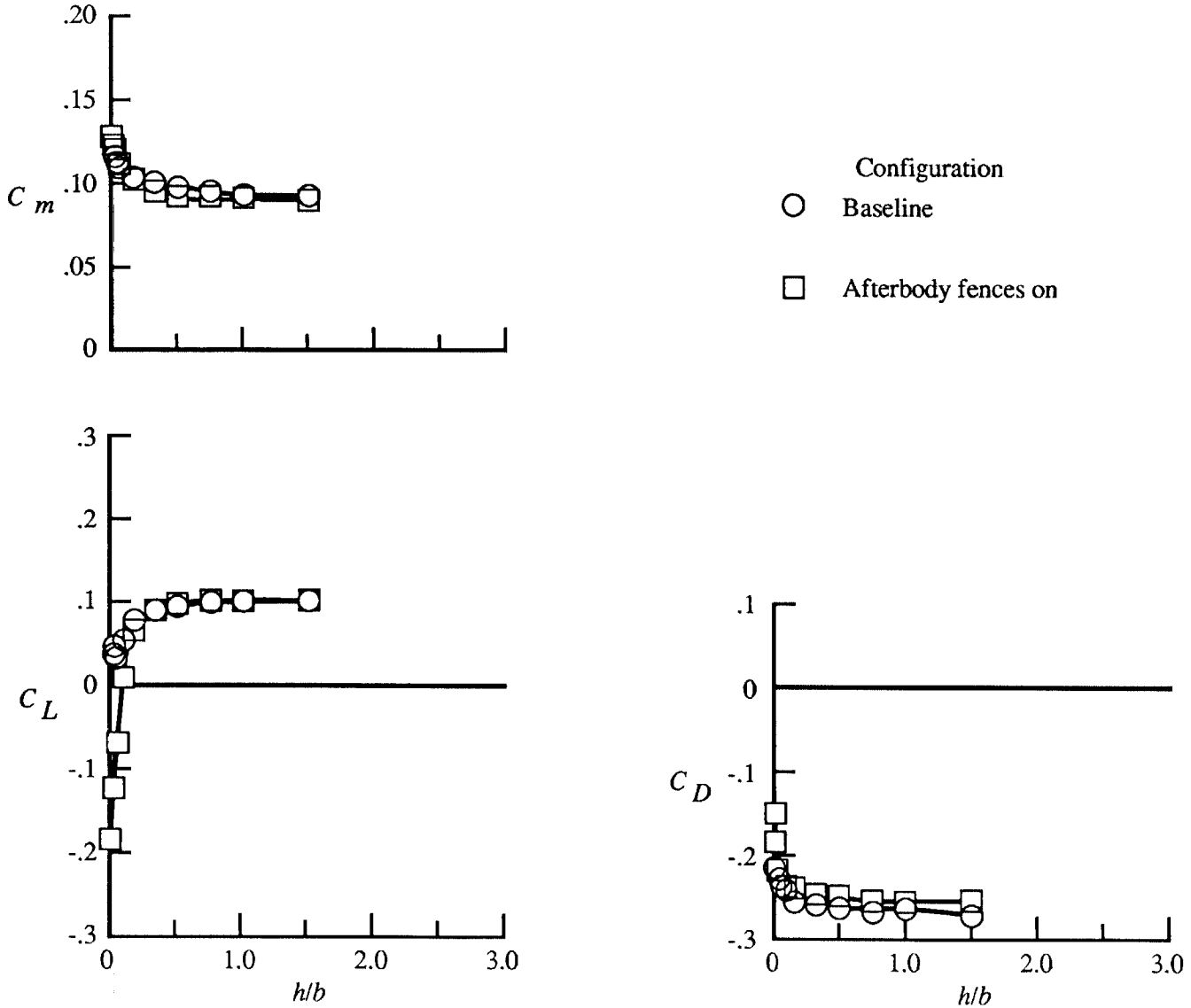

Figure 20. Effects of afterbody fences on longitudinal aerodynamics. $\alpha = 12°$; $C_T = 0.4$; $q_\infty = 40$ psf.

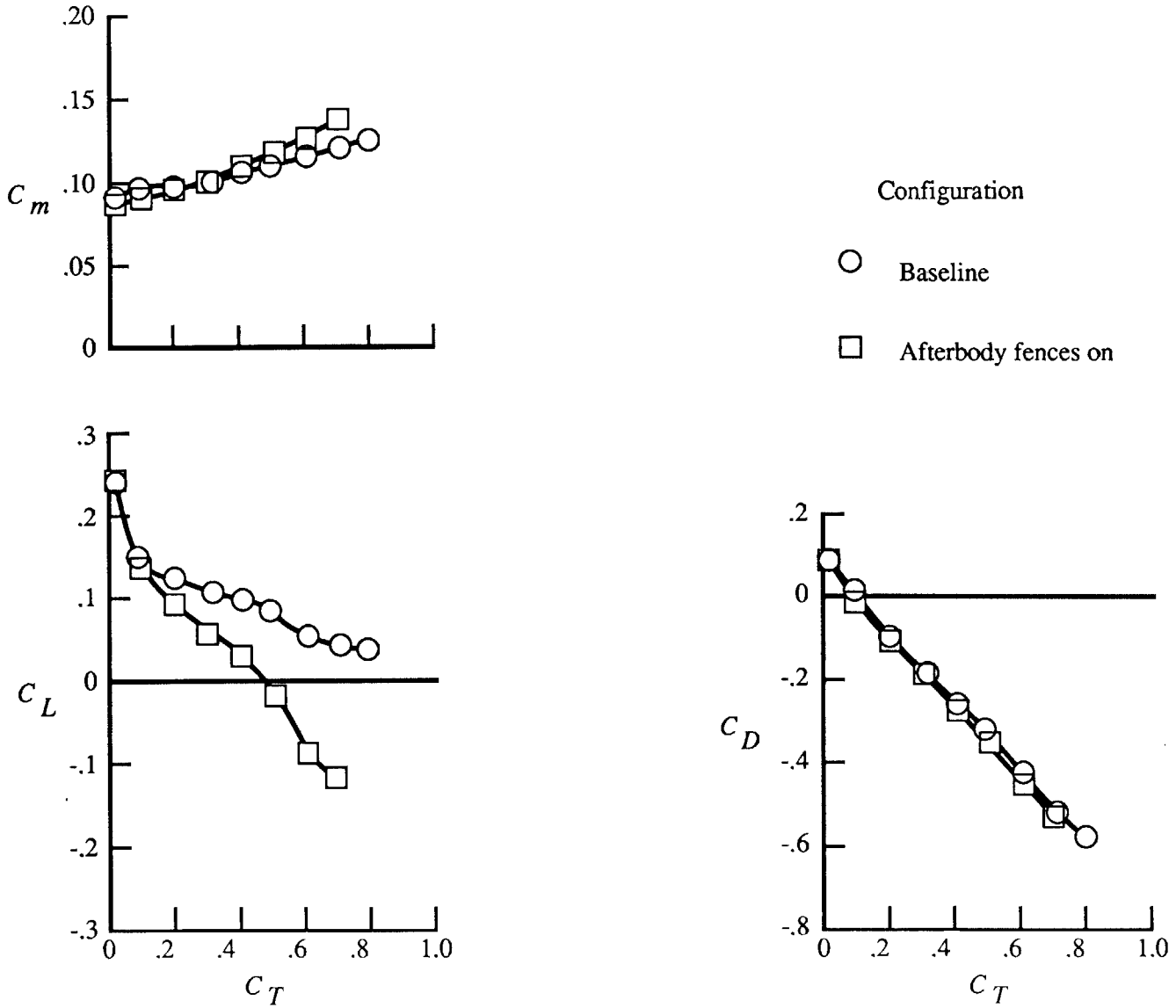

Figure 21. Effects of thrust coefficient variation in ground effect with afterbody fences on. $\alpha = 12°$; $h/b = 0.08$; $q_\infty = 20$ psf.

(a) Baseline.

(b) Fences on.

Figure 22. Flow visualization illustrating effects of afterbody fences on exhaust flow. $\alpha = 12°$; $C_T = 0.2$; $h/b = 0.04$.

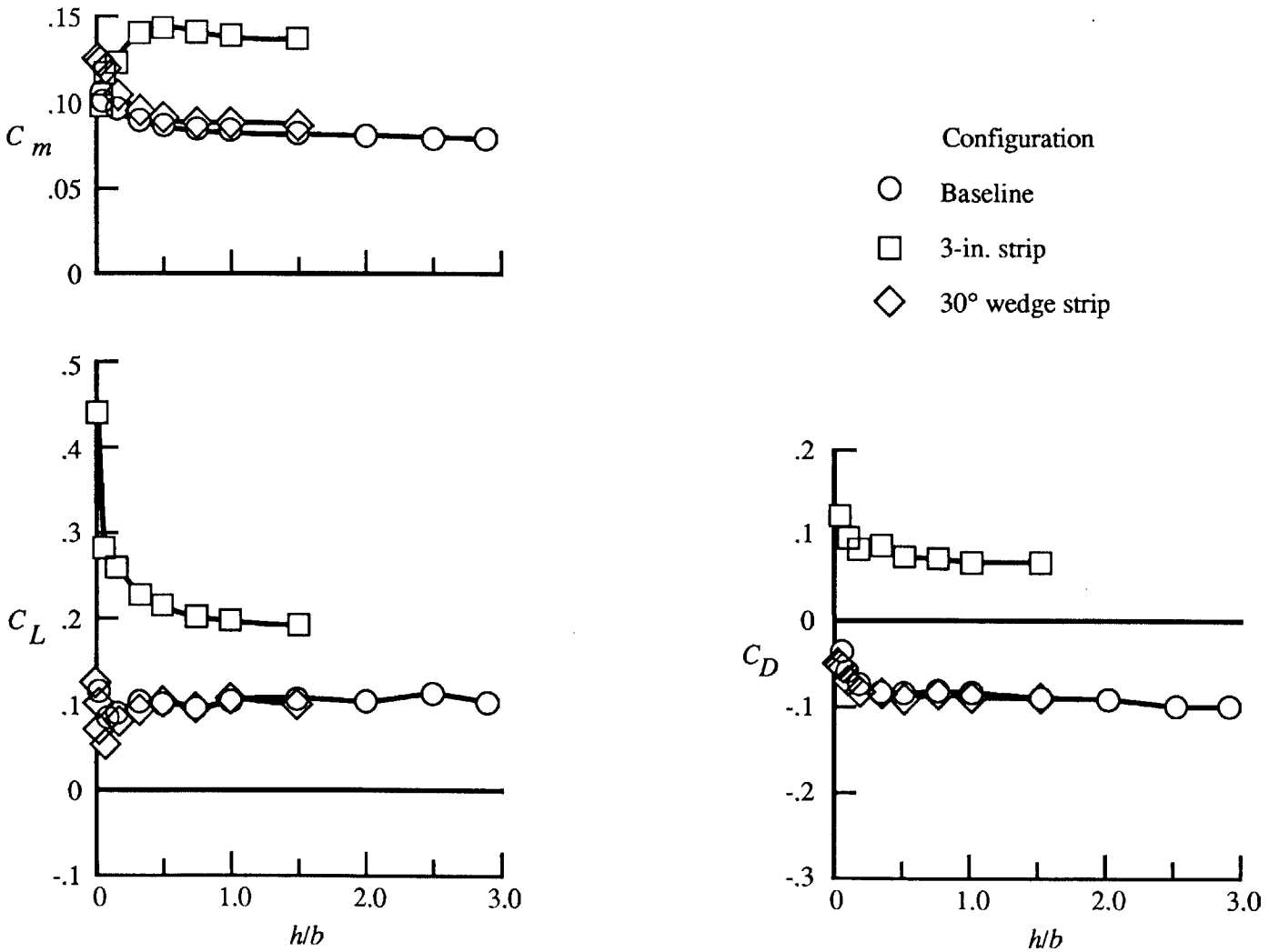

Figure 23. Effects of exhaust flow deflectors on longitudinal aerodynamics. $\alpha = 12°$; $C_T = 0.2$; $q_\infty = 40$ psf.

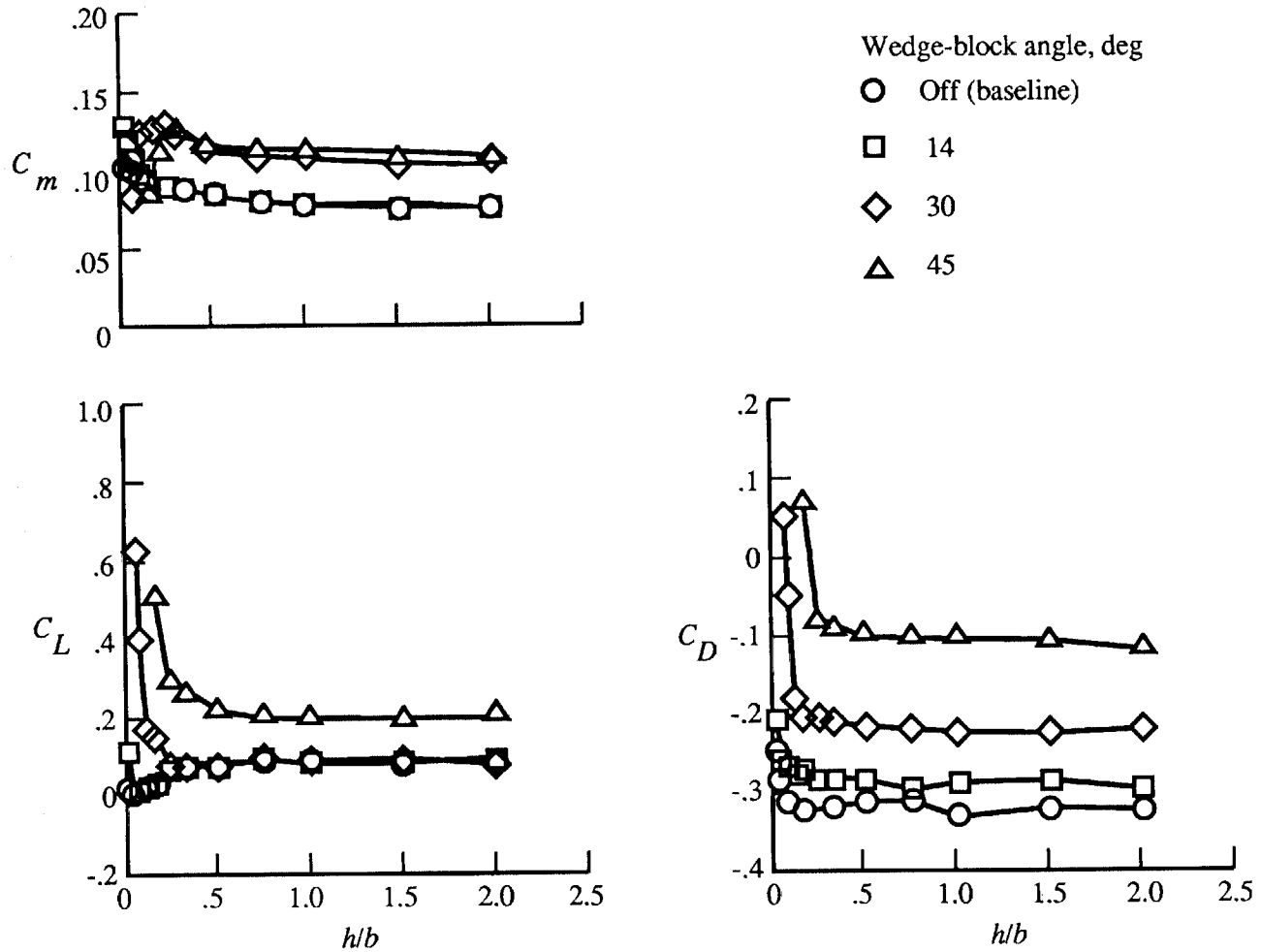

Figure 24. Effects of variation in afterbody wedge-block angle with wedge blocks in forward location. $\alpha = 12°$; $C_T = 0.4$; $q_\infty = 30$ psf.

(a) Side view. $h/b = 0.75$.

(b) Top view. $h/b = 0.21$.

Figure 25. Exhaust flow visualization with 45° wedge block in forward location. $\alpha = 12°$; $C_T = 0.4$; $q_\infty = 30$ psf.

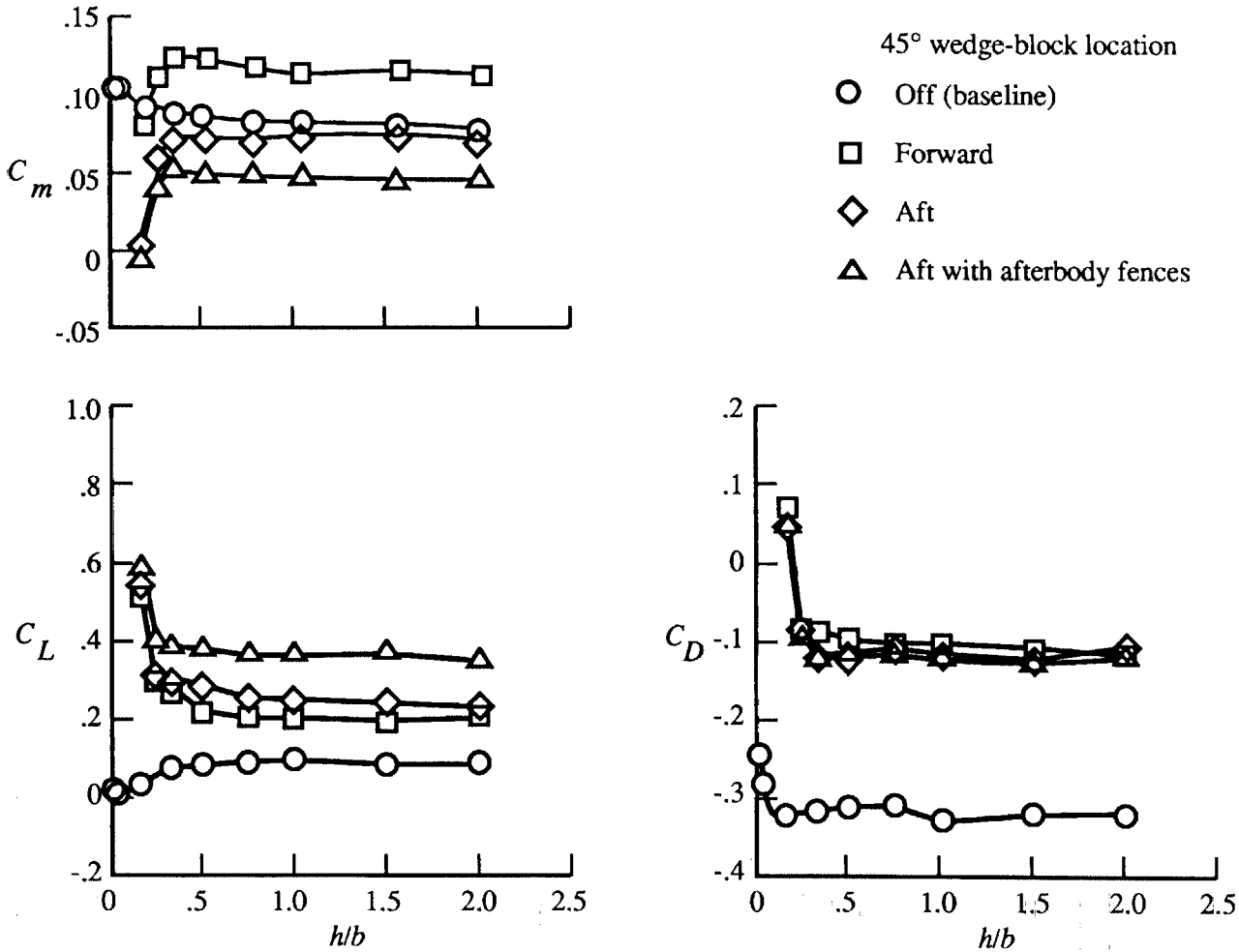

Figure 26. Effects of variation in afterbody wedge-block location. $\alpha = 12°$; $C_T = 0.4$; $q_\infty = 30$ psf.

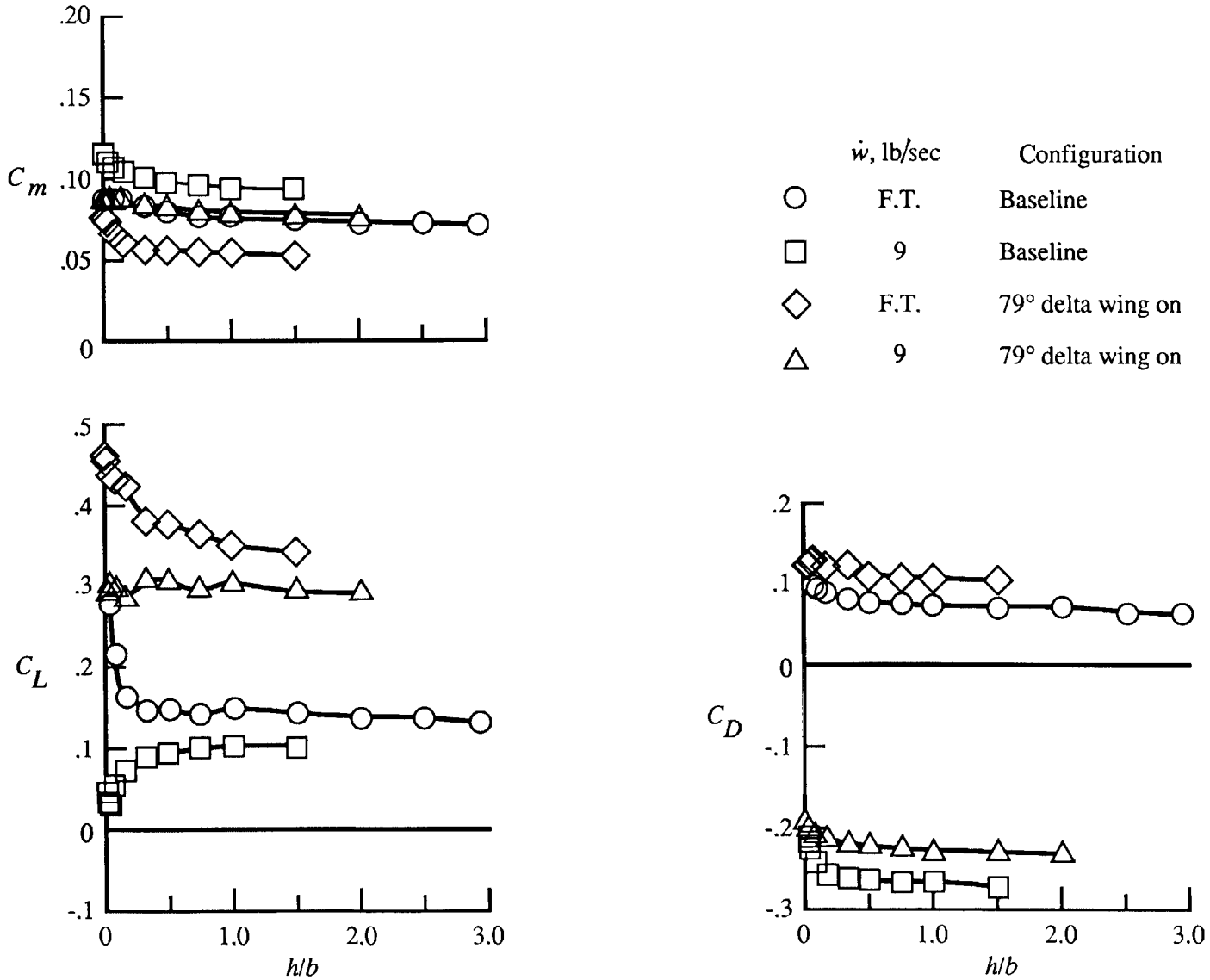

Figure 27. Ground effects data for 79° delta wing configuration. $\alpha = 12°$; $q_\infty = 40$ psf.

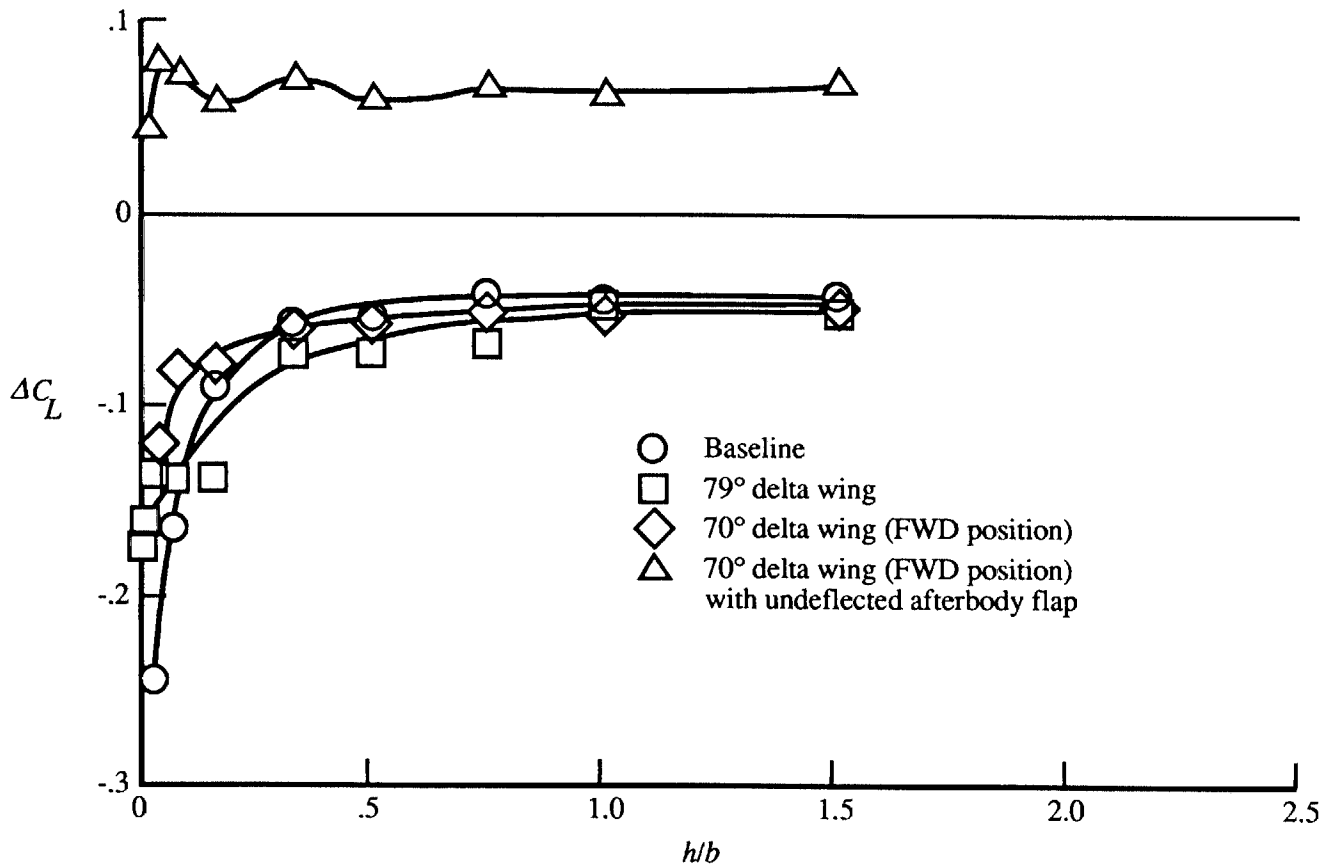

Figure 28. Incremental lift coefficient data illustrating power-on effects of delta wings and afterbody flap. $\alpha = 12°$; $\dot{w} = 9$ lb/sec.

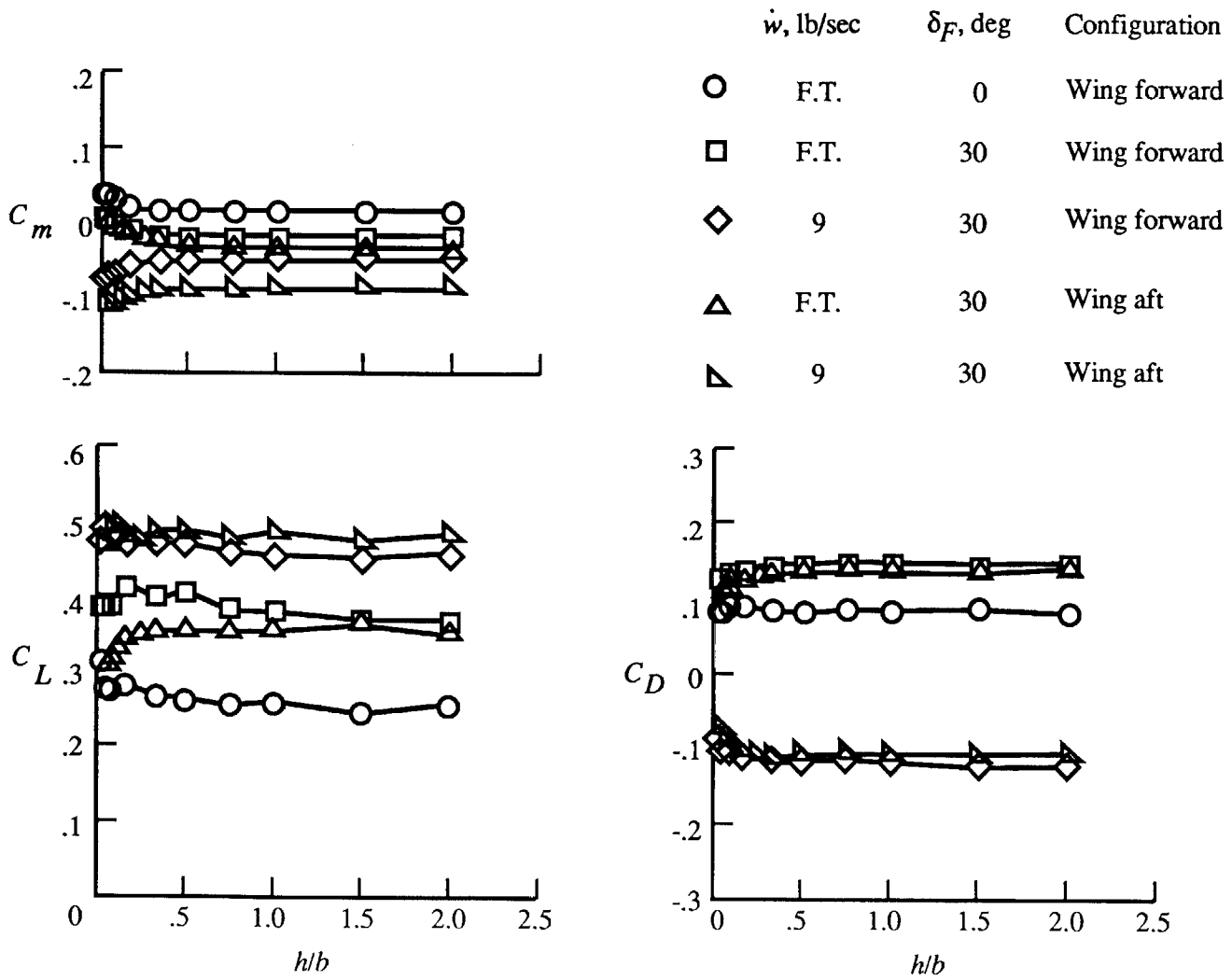

Figure 29. Effects of longitudinal wing position. 70° delta wing; $\alpha = 12°$; $\delta_{ABF} = 0°$; $q_\infty = 30$ psf.

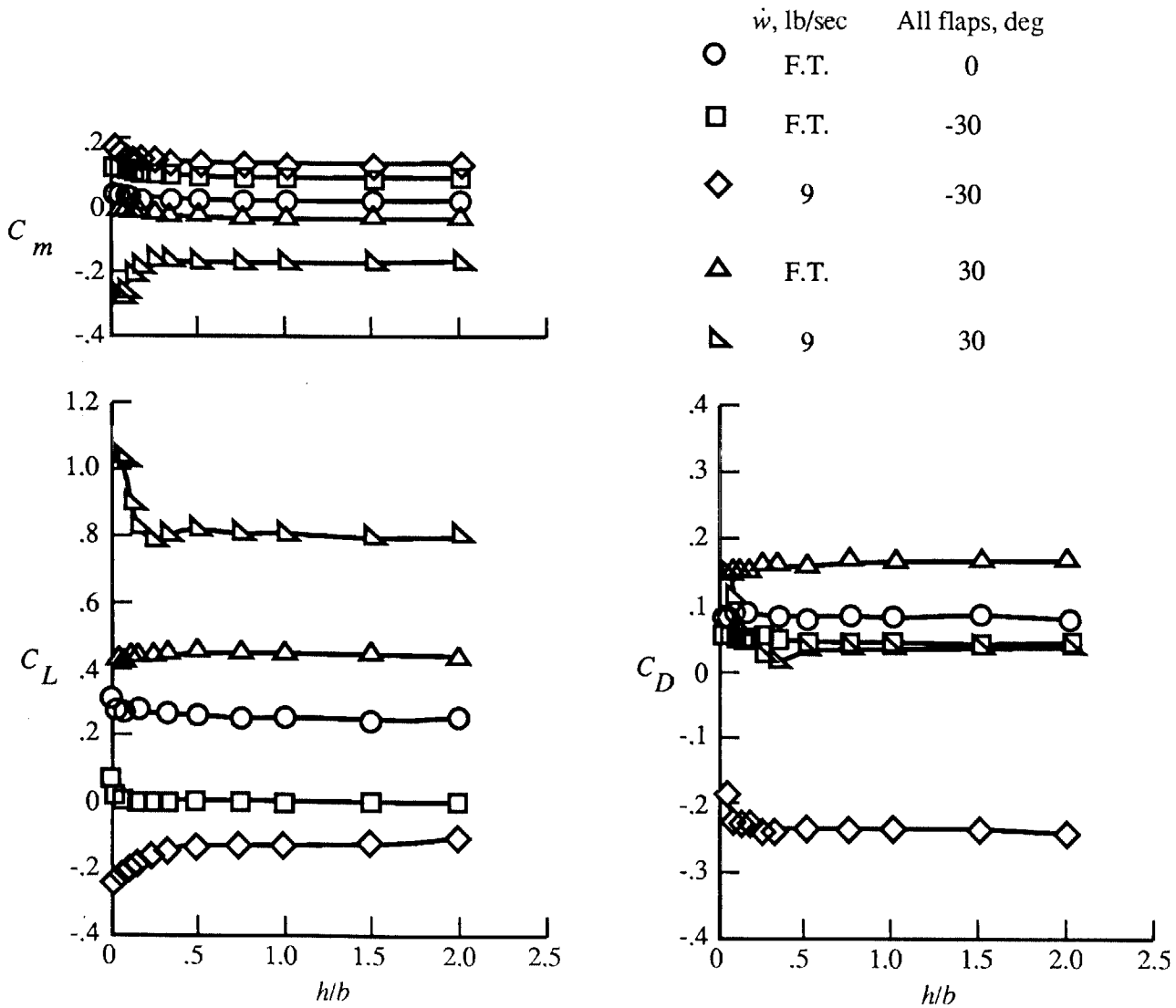

(a) Longitudinal data.

Figure 30. Effects of all flaps deflected. 70° delta wing in forward position; $\alpha = 12°$; $q_\infty = 30$ psf.

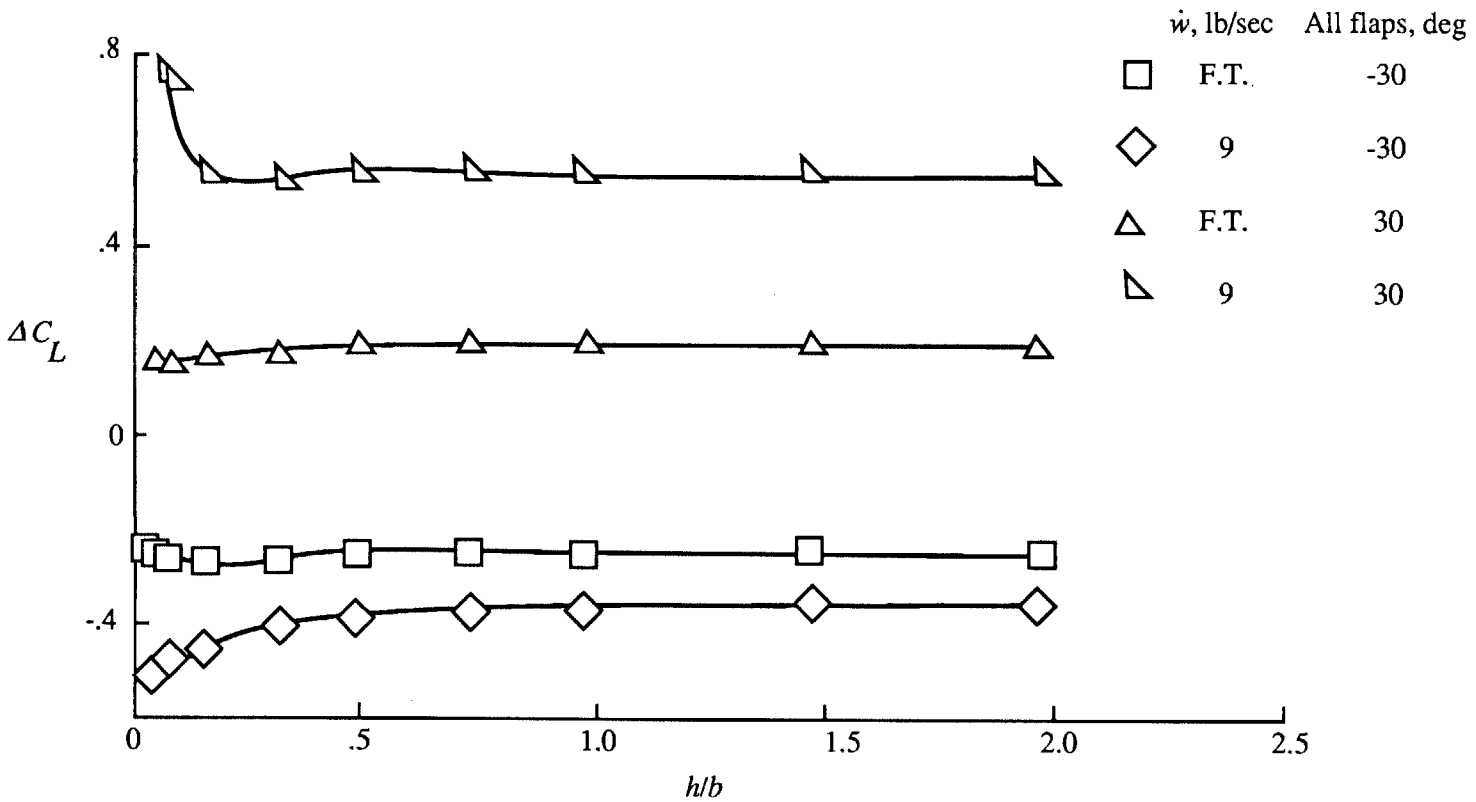

(b) Incremental lift coefficient data.

Figure 30. Concluded.

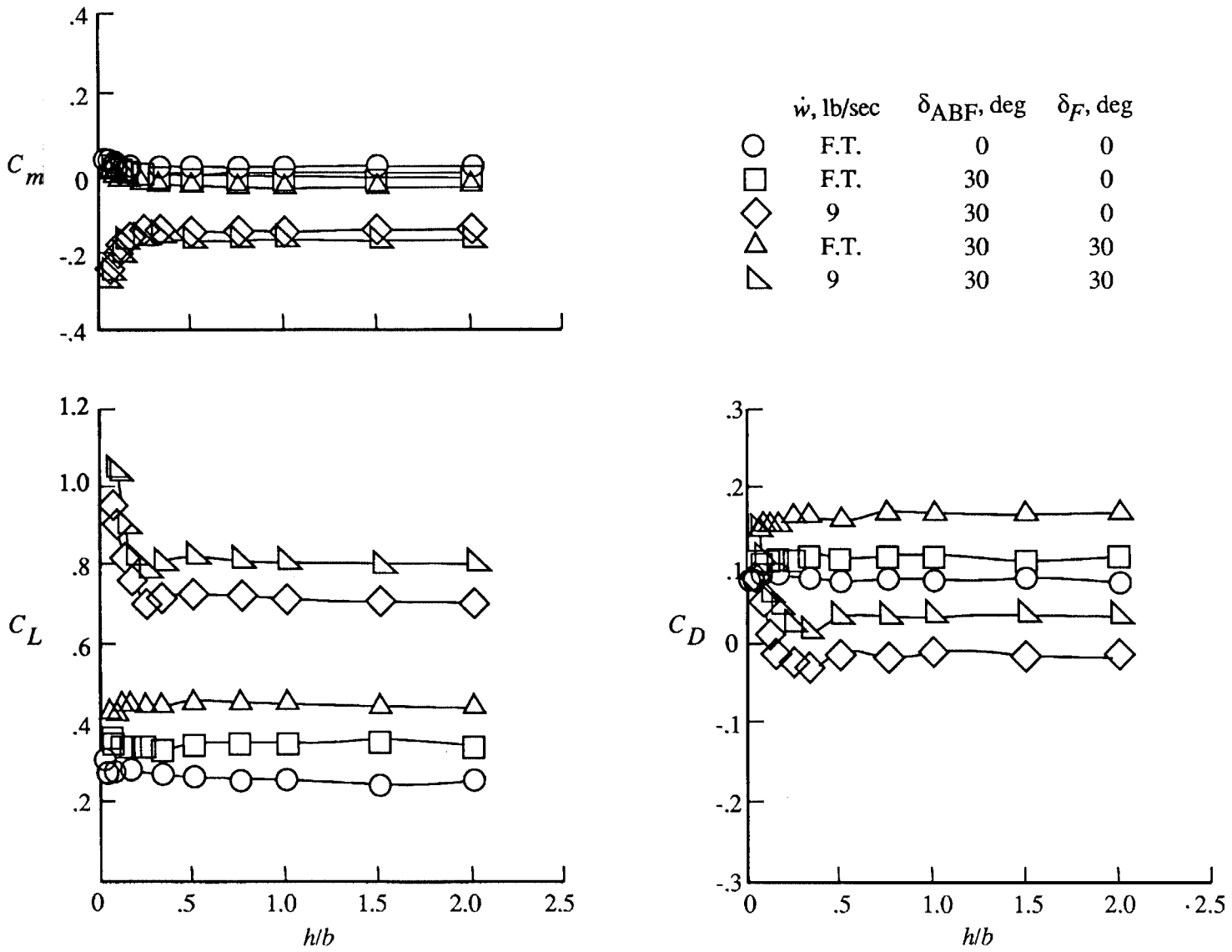

(a) Longitudinal data.

Figure 31. Independent effects of flap deflections. 70° delta wing in forward position; $\alpha = 12°$; $q_\infty = 30$ psf.

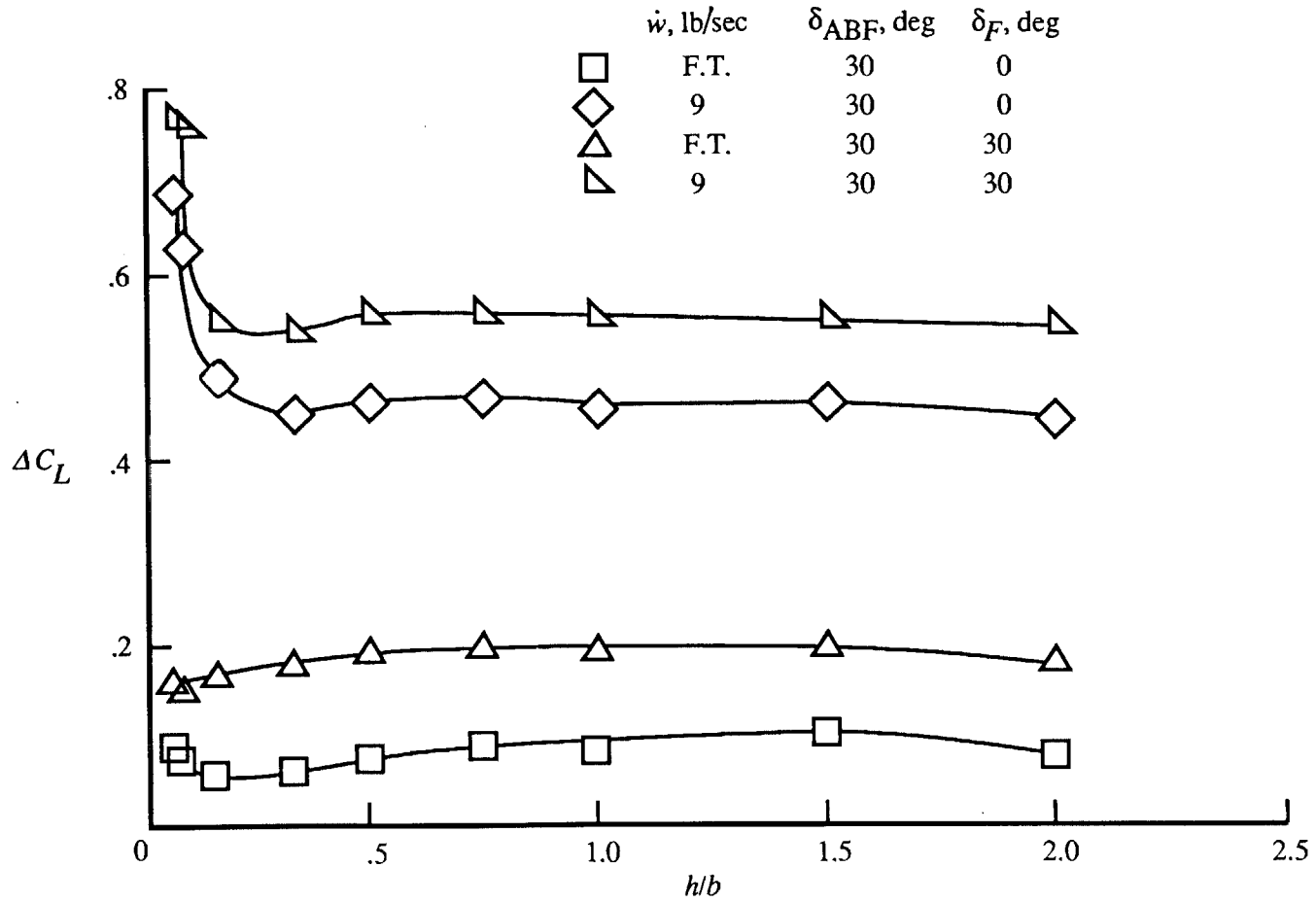

(b) Incremental lift coefficient data.

Figure 31. Concluded.

NASA
National Aeronautics and Space Administration

Report Documentation Page

1. Report No.	2. Government Accession No.	3. Recipient's Catalog No.
NASA TP-3092		

4. Title and Subtitle	5. Report Date
Ground Effects on the Low-Speed Aerodynamics of a Powered, Generic Hypersonic Configuration	May 1991
	6. Performing Organization Code
7. Author(s)	8. Performing Organization Report No.
Gregory M. Gatlin	L-16861
9. Performing Organization Name and Address	10. Work Unit No.
NASA Langley Research Center Hampton, VA 23665-5225	763-01-31-22
	11. Contract or Grant No.
12. Sponsoring Agency Name and Address	13. Type of Report and Period Covered
National Aeronautics and Space Administration Washington, DC 20546-0001	Technical Paper
	14. Sponsoring Agency Code

15. Supplementary Notes

16. Abstract

A study was undertaken in the NASA Langley 14- by 22-Foot Subsonic Tunnel to determine the low-speed aerodynamic characteristics of a powered, generic hypersonic configuration in and out of ground effect. The model was a simplified configuration consisting of a triangular-wedge forebody, a rectangular midsection that housed the flow-through, ejector-type propulsion simulation system, and a rectangular-wedge afterbody. Additional model components included a delta wing, a rectangular-wedge forebody, inlet fences, exhaust flow deflectors, and afterbody fences. Aerodynamic force and moment data were obtained over an angle-of-attack range from $-4°$ to $18°$ while the model height above the tunnel floor was varied from 1/4 in. to 6 ft. Variations in free-stream dynamic pressure, from 10 to 80 psf, and in engine ejector pressure yielded a range of thrust coefficients from 0 to 0.8.

17. Key Words (Suggested by Author(s))
Ground effects
NASP
Powered model
Flow visualization
Low speed

18. Distribution Statement
Unclassified—Unlimited

Subject Category 02

19. Security Classif. (of this report)	20. Security Classif. (of this page)	21. No. of Pages	22. Price
Unclassified	Unclassified	60	A04